



Failure mechanism of a massive fault–controlled rainfall–triggered landslide in northern Pakistan

Abstract A massive landslide occurred in Domeshi area, District Muzaffarabad, Pakistan, in two distinct phases: an initial movement on August 1, followed by complete failure on August 4, 2023. The landslide movement persisted for 96 h, with a runout distance of 500 m. The event destroyed numerous residential structures, impacting multiple families, and causing extensive damage to cultivated land and road infrastructure. To comprehensively understand the failure mechanisms, a detailed study was undertaken, encompassing site investigations, unmanned aerial vehicle (UAV) photography, geotechnical and geophysical investigations, petrographic analysis, kinematics, and numerical simulations. The field evidence indicates that the active deformation along the Jhelum Fault (JF) within the landslide's main body weakened the surrounding rock formations. Intense rainfall saturated pre-existing fractures, creating critical zones of weakness. Highly plastic clays along fault plane contributed significantly to volume changes, especially during and after rainfall events. Kinematic analysis identified bedding joints as prevalent failure planes for planar sliding. Geophysical survey revealed a layer of unconsolidated material extending 25–30 m below the landslide's scarp, accompanied by various fractures, including a deep fracture (i.e., JF) up to 300 m depth. Petrographic investigations showed microfractures, micro faults, and intragranular mineral breakage, indicative of intense tectonic stresses. Slope stability analysis indicated factors of safety (FoS) and strength reduction factor (SRF) less than 1, suggesting the potential for further failure in the lower sections of the landslide. Multiple factors, including slope geometry, active tectonics, material composition, and anthropogenic factors (i.e., slope loading and cutting for road and building construction, improper drainage distribution), contributed to the landslide's occurrence, however, the rainfall emerged as the primary triggering event.

Keywords Fault controlled landslide · Failure mechanism · Rainfall · Geophysical investigation · Northern Pakistan

Introduction

The climate-induced cascading geohazards have adverse impacts on the infrastructure, population, and ecosystem of the region (Thomas 2017; Petley et al. 2005; Zhang et al. 2020). Due to global warming, significant changes in the monsoon rain have been observed in the mountainous terrain of the Himalayas (Sabin et al. 2020). The landslides, debris flows, and glacial outburst floods (GLOFs) are mainly triggered due to heavy rainfall on hilly terrains,

and can destroy transportation networks, infrastructure, and even entire communities (Peng et al. 2023). Natural disasters severely impact the developing countries causing significant human casualties and economic loss (Lacroix et al. 2020; Panwar and Sen 2019). The destructive potential of landslides has been increased with increasing intensity of severe weather conditions (Cappelli et al. 2021; Sim et al. 2022; Gómez et al. 2023). Landuse practices for the expansion of human settlements in hazardous and vulnerable areas further enhances the risk of landslide hazards (Jiang et al. 2021; Santangelo et al. 2023).

A small magnitude earthquake can trigger a landslide in hilly areas (Hufschmidt et al. 2005). The northern parts of Pakistan are characterized by active tectonics, fragile geology, and diverse topography which make them highly vulnerable to landslides (Basharat et al. 2021; Riaz et al. 2018). Accumulated and antecedent rainfall patterns further intensify the landslide frequency in the region (Riaz et al. 2019). Therefore, interplay of climatic conditions and seismic activities compromise slope stability, making the Himalayas landslide susceptible region. One of the most devastating seismic event (2005 Kashmir earthquake) caused 87,000 casualties out of which 26,000 were directly or indirectly caused by the earthquake triggered landslides (Basharat et al. 2021). These landslides also severely affected the public infrastructure including roads, houses, water supply, electrical transmission lines, and rural pathways (Khattak et al. 2010; Riaz et al. 2023). After this mega event, a continued landslide activity has been observed due to heavy rainfall such as Danna Sahoter Landslide (Khan et al. 2021), Shahkot Landslide (Ahmed et al. 2021), Donga Kass Landslide (Riaz et al. 2019), Lohar Gali Landslide, Nauseri Landslide, and Langerpura Landslide (Riaz et al. 2023).

A massive Domeshi Landslide occurred recently in August 2023 near Rara village, District Muzaffarabad, Pakistan. The landslide resulted in the destruction of dozens of houses, metaled road, agricultural land, electric poles, and severely damaged various buildings in vicinity of the landslide. To analyze the causative factors and triggering mechanism of landslide, an understanding of the geological, geotechnical, morphological, and ground water parameters is essential (Tang et al. 2018). The integration of geophysical, geotechnical, petrographic, numerical, and kinematic analyses play a crucial role in investigating landslides (Khan et al. 2021; Mezerreg et al. 2019). Therefore, an integrated approach using these parameters was adopted to understand the failure mechanism of Domeshi Landslide. Geophysical techniques offer insights into the landslide's geometry, subsurface materials,

potential slip surface depth, and tectonic features. The geophysical methods are advantageous due to effective digital data acquisition, processing and interpretation (Pasierb et al. 2019). The electrical resistivity tomography (ERT) has been traditionally used as a geophysical technique for landslide studies. The audio-magneto-telluric (AMT) method has been recently used due to its ability to demarcate deep geological structures and subsurface water conditions (Yusuf et al. 2022; Cygal et al. 2021), making it particularly suitable for studies like the fault-controlled Domeshi Landslide. Geotechnical investigations provide essential data on material strength and behavior under stress, including shear strength parameters and soil moisture conditions, which are pivotal for slope stability analysis (Kinde et al. 2024). In the complex geological environment, traditional geotechnical methods must be coupled with numerical modelling for analyzing real case scenarios of the landslide stability (Truty et al. 2009; Wysokiński 2011; Ozbay and Cabalar 2015; Xu and Yang 2018). These methods provide potential failure mechanism including slip surface and factor of safety (FoS) representing an equilibrium between the slope stabilizing and destabilizing forces. Numerical tools such as the limit equilibrium method (LEM), finite difference method (FDM), boundary element method (BEM), and finite element method (FEM) have been used by researchers for the analysis of slope stability problems (Griffiths and Lane 1999; Cheng et al. 2007; Liu et al. 2015; Stianson et al. 2015; Mebrahtu et al. 2022). These methods, i.e., FDM, BEM, LEM, and FEM, can simulate and assess landslide behavior and stability (Pourkhosravani and Kalantari 2011). Due to progressive failure modeling capabilities, FEM is widely used to model slope stability (Mebrahtu et al. 2022). Shear strength reduction (SSR) is one of the most popular methods for slope stability analysis by FEM and broad applications exist in literatures (Griffiths and Lane 1999). Various authors have compared the results of slope stability analyses between different LEM and FEM (Hammah et al. 2004; Khabbaz et al. 2012; Vinod et al. 2017; Zein and Karim 2017), pointing to a good consistency between LEM and FEM on simple geometries with homogenous material, but highlighted an overestimation of the slope stability using LEM for complex geometries, with heterogeneous material. Hammah et al. (2004) proposed FEM using SSR factor as a robust approach for slope stability. The stability conditions of the rock slope cannot be expressed by a single method, so different methods should be compared (Sari 2019). For better understanding of triggering mechanism of Domeshi Landslide, numerical simulations on slope stability using FDM, LEM and FEM combined with SSR technique with Mohr–Coulomb failure criteria was carried out along with comparison among these methods. Kinematic analysis is a useful tool for geometric evaluation of slopes and to assess the probability of various kinds of failures (such as planar, toppling, and wedge failures) based on unfavorably oriented discontinuities (Rahman et al. 2023). The petrographic analysis evaluates the mineralogy, grain fabric, and micro discontinuities of the rocks. This helps to deduce valuable information on effects of tectonic stresses and diagenetic history affecting the strength and durability of rocks in the area, ultimately affecting the stability of slopes (Askaripour et al. 2022). The comprehensive integration of these approaches provides valuable information regarding Domeshi Landslide failure

mechanisms enabling informed decision-making and mitigation strategies.

Study area

The northern regions of Pakistan are highly susceptible to landslides (Riaz et al. 2022; Kiani et al. 2022). The increased landslide activity in the monsoon season suggests that rainfall is a prominent triggering factor causing over half of the documented landslide incidents globally (Gariano and Guzzetti 2016). A similar trend is observed in Pakistan that cause severe damage and loss of life every year (Shabbir et al. 2023; Khan et al. 2021; Haque et al. 2019). Pakistan has suffered economic losses of approximately \$3.8 billion from 1999 to 2018 due to the climate change impacts (Eckstein et al. 2021).

Domeshi Landslide is situated in the village of Domeshi, approximately 10 km south of Muzaffarabad city located along the right bank of the Jhelum River. Muzaffarabad District itself lies within the territorial bounds of Azad Jammu & Kashmir (AJ&K), positioned about 140 km northeast of Islamabad, the capital city of Pakistan (Fig. 1). The Domeshi Landslide is a destructive landslide which initiated on the 1st of August 2023 and the complete failure occurred on the 4th of August 2023. The landslide is accessible through Muzaffarabad-Kohala road via Ambore and Domeshi bridges (Fig. 1). In 2023, Pakistan experienced significantly heightened precipitation levels, particularly in July, marking a notable deviation from typical rainfall patterns. Throughout the month, Pakistan encountered 4–5 widespread heavy to very heavy rainfall episodes, contributing to an overall above-average precipitation rate of 70% for the country as a whole. This exceptional rainfall propelled July 2023 to rank as the 9th wettest July on record, with the previous record set at 177.80 mm in 2022. This data underscores the significant and unprecedented precipitation levels that Pakistan experienced, particularly in July 2023 (Fig. 2).

Tectonic and geological setting

The study area lies in the southwestern part of the Hazara-Kashmir Syntaxis (HKS), in the Sub-Himalayan division of the NW Himalayas, Pakistan (Fig. 3). The rocks in the area have undergone intense deformation, especially the western limb of HKS is highly deformed and truncated by a series of faults, most importantly the Jhelum Fault (JF) (Ali et al. 2015; Safi et al. 2021). JF is a NS trending left-lateral strike-slip fault with occasional thrust component, that runs along the Jhelum River from Muzaffarabad to Kohala (Monalisa and Khawaja 2004). It separates the Precambrian Hazara Formation in the west from the Miocene Murree Formation in the east in an area between Muzaffarabad and Rara and continues south between the Murree Formation and Mesozoic Rara Formation of Greco, 1989 (Turab 2012). Generally, rock formations ranging from Precambrian to Recent are exposed in the area (Fig. 3). Specifically in the study area, the exposed rock formations are the Precambrian Hazara Formation and Miocene Murree Formation. The Hazara Formation dominantly consists of slates; however, in the studied section, it comprises of quartzite, dolomitic limestone, and minor graphitic phyllites (Fig. 4; Shahzad et al. 2024).

Within the Domeshi Landslide, two different types of quartzite were found in the head and lower parts of the scarp along the fault. The lower unit consists of very light grey to off-white, fine-grained and highly fractured quartzite (Fig. 5c) while the upper

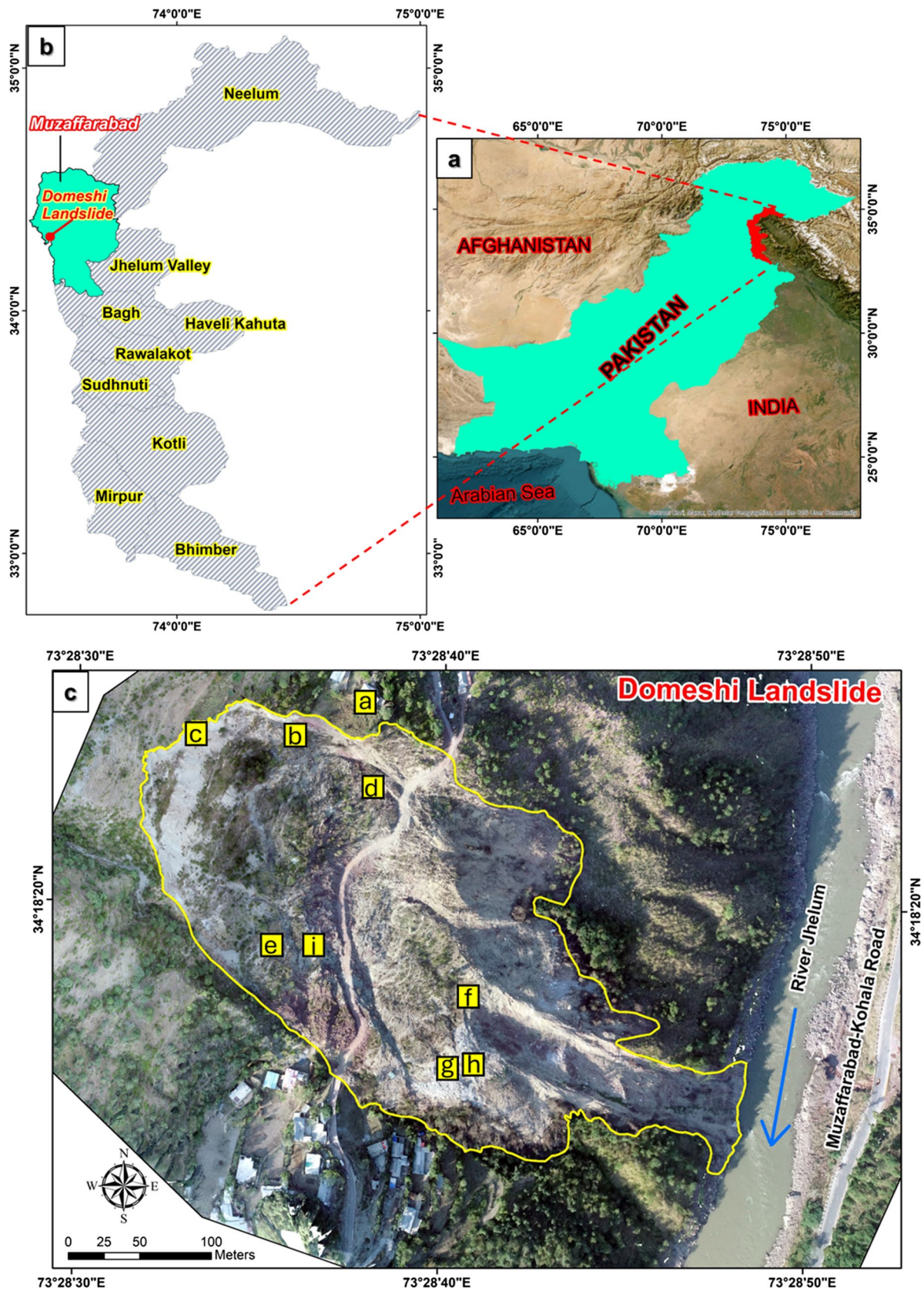


Fig. 1 Geographic representation of the landslide area: **a** Position of AJ&K within the map of Pakistan. **b** AJ&K map highlighting the location of the Domeshi Landslide within District Muzaffarabad. **c** Aerial photograph depicting the massive Domeshi Landslide triggered in August 2023. Rectangles representing the location of field photographs (Fig. 6) of landslide

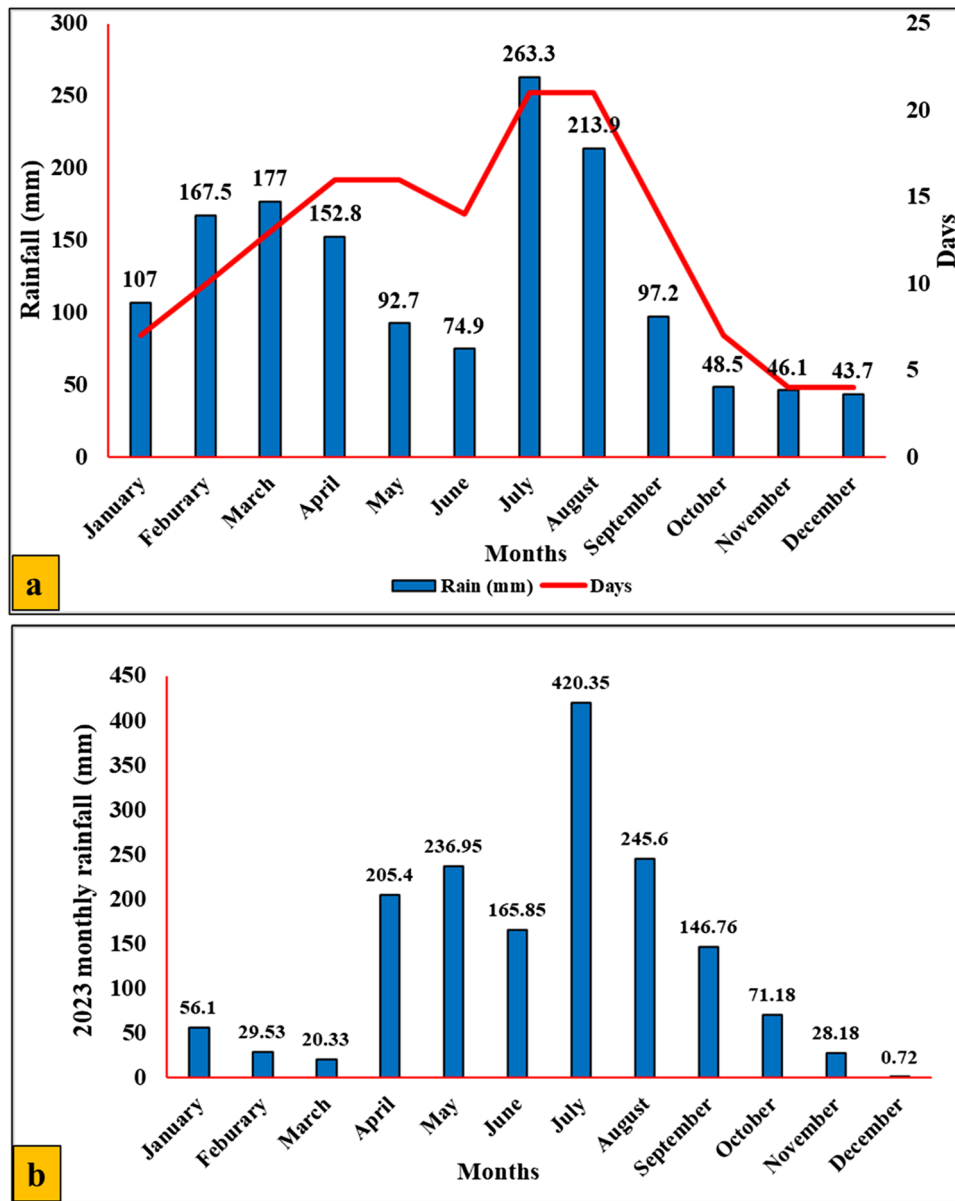


Fig. 2 **a** Average monthly rainfall of Muzaffarabad from 2000 to 2022. **b** Monthly rainfall data of Muzaffarabad from January to December 2023 showing highest rainfall of 420 mm in the month of July

unit consists of light to dark greenish grey fresh colour with rusty brown weathered/altered colour at places, dense, medium to coarse-grained quartzite (Figs. 4 and 5). The dolomitic limestone is exposed at the crown and top parts of the scarp (Fig. 5b). It is characterized by light to medium grey fresh and light brownish grey weathered colour, fine to medium grained, thin to medium bedded with alternate horizontal, and wavy microbial algal lamination. Generally, the Murree Formation is characterized by cyclic deposition of sandstone, mudstone, and shales. However, at the landslide location mainly reddish and maroonish clays are exposed with minor sandstone patches adjacent to the landslide (Fig. 5d; Shaheen et al. 2023). Along the fault plane within the landslide, the rock units

are highly crushed and sheared into gouge and brecciated material within a zone of 1.5 m showing cataclastic deformation.

Material and methods

The study adopts a comprehensive methodology integrating various field, laboratory, and numerical modeling techniques to understand the triggering mechanisms and assess the stability of the affected area for the Domeshi Landslide. Field investigations comprise of detailed geomorphological mapping facilitated by unmanned aerial vehicle (UAV) surveys, allowing for the identification of key landforms and features indicative of landslide activity. Strength and stiffness parameters of landslide as well as intact part

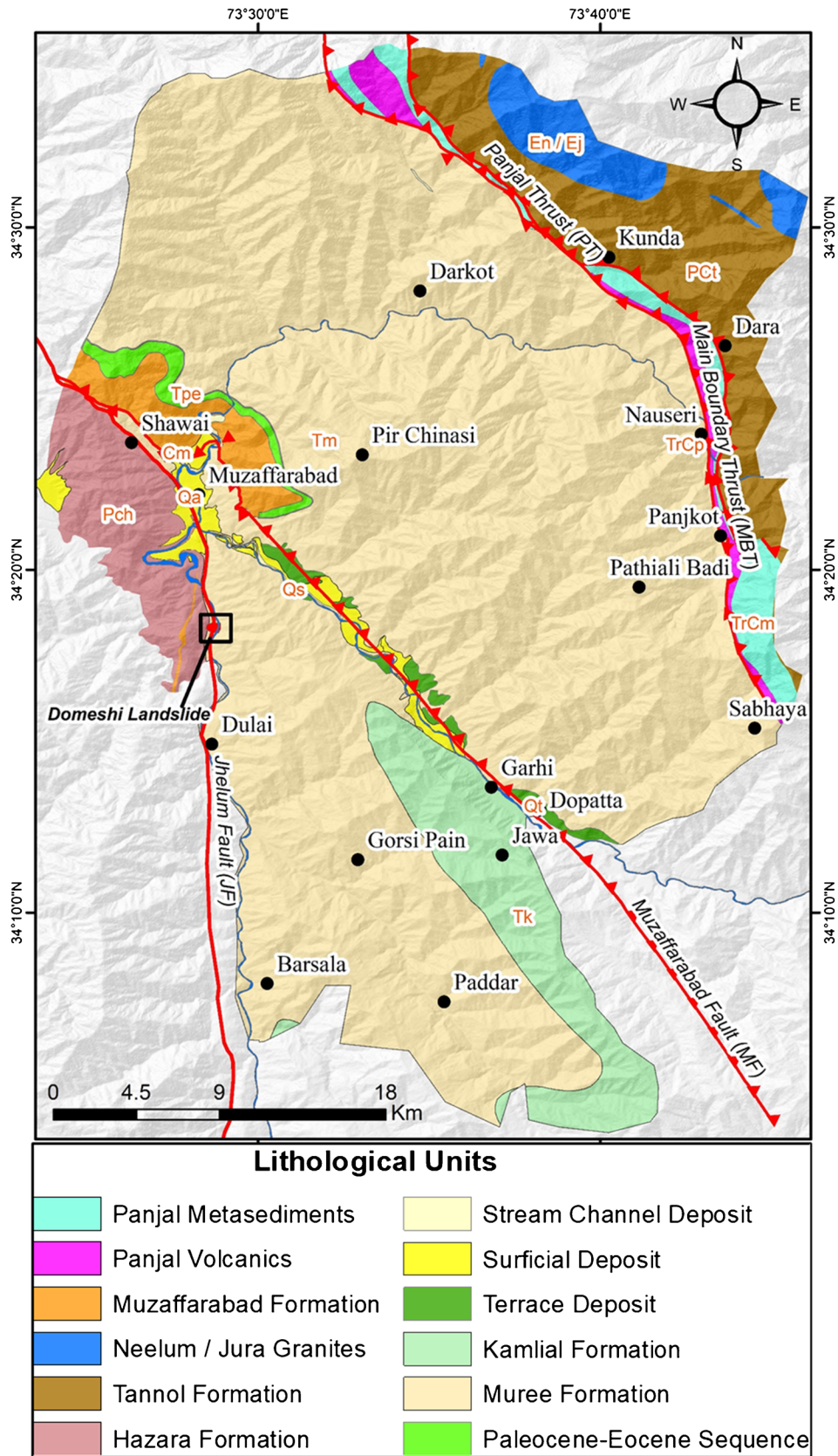


Fig. 3 Geological Map of the district Muzaffarabad (Adopted from Riaz et al. 2023). Rectangle shows the location of Domeshi Landslide; Jhelum Fault is running within the landslide body

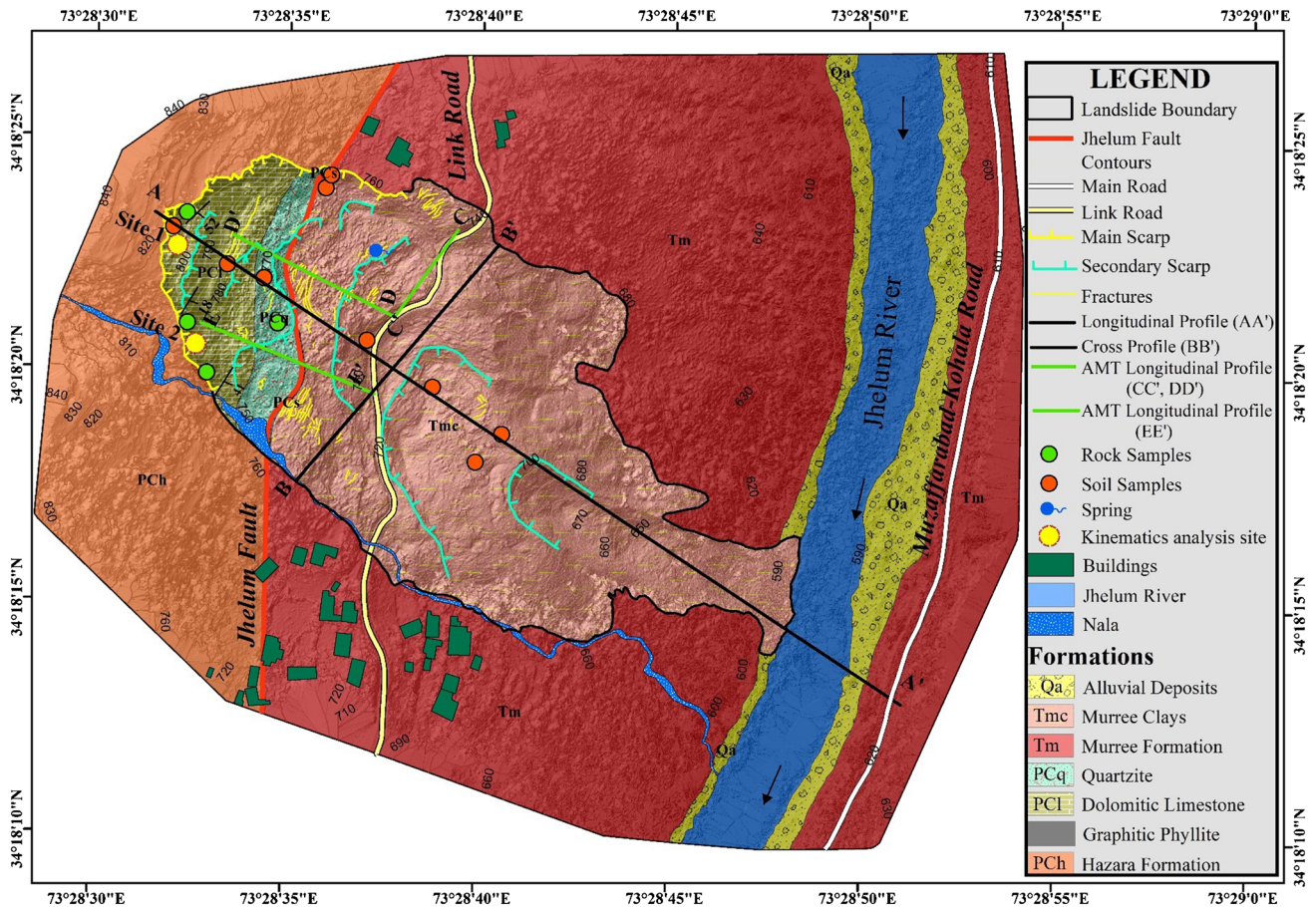


Fig. 4 Geological and geomorphological map of Domeshi Landslide representing various rock units and morphological characteristics, location of soil and rock samples, landslide longitudinal (A-A'), cross sectional (B-B') and geophysical profiles (C-C'; D-D'; E-E') orientation

were collected using in-situ testing. Geotechnical data collection involves the collection and analysis of soil and rock samples within the landslide zone, providing insights into soil properties and shear strength parameters crucial for stability assessment. AMT surveys were used to delineate subsurface geology and structures as well as the potential failure surfaces of the landslide. FLAC and Slope/W software were used for FDM and LEM respectively for estimation of FoS and potential slip surface incorporating field- and laboratory-derived geotechnical parameters. Strength reduction FEM technique was performed using RS2 software. Kinematic analysis was performed based on discontinuity data from the landslide site using Dips software.

Field study

The necessary data and sampling for various designed parameters were collected by conducting multiple field visits to the landslide site between August 2023 and April 2024. Field investigations entail detailed geomorphological mapping facilitated by UAV surveys. Eight soil and four rock samples were collected for detailed laboratory geotechnical analysis. AMT survey was also performed in the field. For kinematic analysis, a discontinuity survey was performed. Geomorphological mapping was facilitated using laser distance

measurement (e.g., RIGEL-LD05e) providing precise measurements of both angles and distances. Longitudinal and cross profiles were constructed to examine elevation variations along the length and width of the landslide area.

Geotechnical experimentation

The geotechnical experimentation includes particle size distribution, consistency limits, laboratory compaction tests, specific gravity, field density, and shear strength parameters for soil and rock. The particle size analysis was carried out according to the ASTM D6913/D6913M-17. The soil samples were sieved through a stack of sieve set progressively finer from top to bottom with a pan at the bottom. The soil retained on each sieve was then weighed and a cumulative percentage against each sieve was calculated which represents the percent finer percentage. The passing and retaining percentages of the respective sieve sizes were then plotted on the particle distribution curve to determine the distribution of various size fractions.

Liquid limit (LL), plastic limit (PL), and plasticity index (PI) were determined according to the ASTM D-4318. LL of soils passing through the No. 40 sieve was determined by using the Casagrande apparatus while the PL test was obtained by rolling the same soil

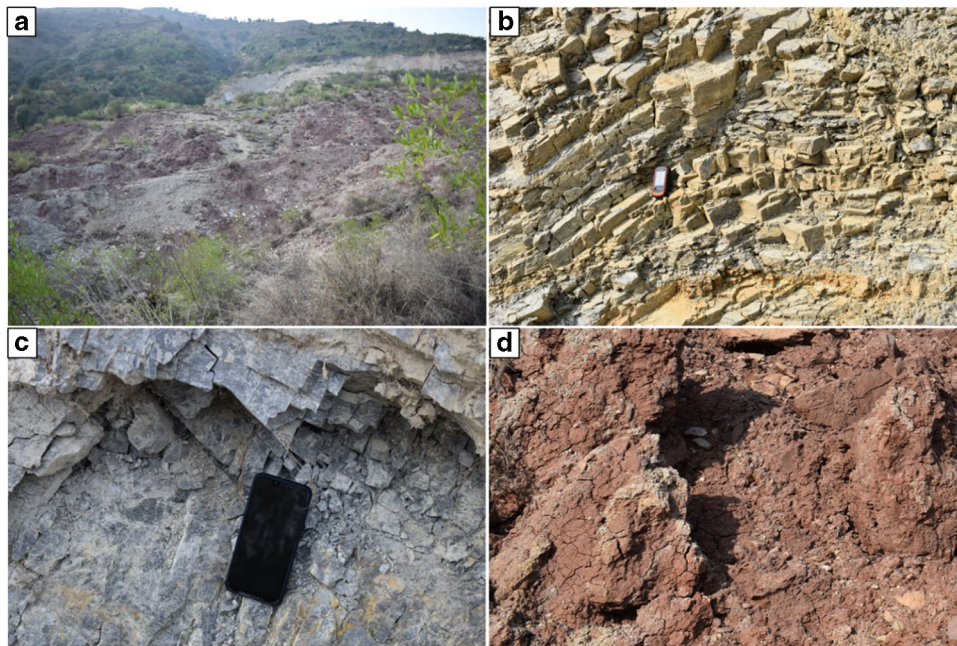


Fig. 5 **a** Photograph showing generalized exposure of various rock units within the landslide. **b** Thinly bedded fractured algal dolomitic limestone of Precambrian Hazara Formation exposed along the scarp of landslide dipping towards SE. **c** Fine grained light grey sheared quartzite of Hazra Formation. **d** Reddish maroon clays of Miocene Murree Formation exposed in the landslide body and toe side

sample into 3-mm-diameter threads until crack initiation. Later on, the PI was computed for the tested soils based on the LL and PL. The transition of soil states from solid to semi-solid, semi-solid to liquid, and finally solid again greatly influenced by the amount of water in a soil mix. These limits indicate the soil's plasticity which in turn characterizes the movement of landslide material (Mous-sadek et al. 2017).

Laboratory compaction tests were employed to evaluate the percent compaction and molding, moisture content required to achieve the soil's engineering characteristics, and for the assessment of the moisture density relationship of the varied-sized soil particles comprising the slope material. The tests were conducted according to the ASTM D1557-12. In this test, soil samples finer than the #4 sieve were compacted in 5 layers in a 4-inch diameter mold with 25 blows of the hammer dropping from a 45 cm height. The procedure was repeated three to five times for each sample and the dry density and moisture content values were recorded. Later on, the maximum dry density (MDD) and optimum moisture content (OPC) were computed by plotting the dry density and water content values on the graph.

The evaluation of shear strength of soil and rock materials is of prime importance for slope stability analysis and suggesting appropriate mitigations (Tiwari and Ajmera 2023). In situ Schmidt hammer test was employed to determine the strength parameters of rock, while a soil penetrometer was used for soil strength determination. Additionally, in-situ vane shear tests were conducted to measure the shear strength of clayey soils. In the current study, the shear strength test of soil has also been performed on the remolded soil samples according to the ASTM D3080/D3080M (Tiwari and Ajmera 2011). The direct shear test was performed in a shear box apparatus by applying vertical stress on the soil sample. The sample

was split into two halves horizontally and then increasing horizontal stress up to the maximum value to generate the horizontal displacement along the failure plane provided. The shear strength of rock is the most critical mechanical property obtained through direct shear box apparatus. After loading the sample in the shear box, two gauges were attached with the upper half of the split box to measure the vertical displacement while one gauge was installed with the lower half of the shear box to measure the horizontal displacement.

To estimate the in-situ density and degree of compaction of the soils, the core cutter method is widely used (Farooq et al. 2015) to confirm the stability and quality of soil layers. The test involves the extraction of a soil core in a cylindrical cutter in the field, by embedding the cylinder into the ground and then measuring its dimensions and calculating its volume. Moreover, the moisture content is calculated to measure the effect of phase changes.

The specific gravity of the soil solids is a vital property to ascertain the soil phase relationships and extent of saturation while it also indicates the density of the soil solid particles. The specific gravity of soils was determined according to ASTM D854. In the laboratory, the specific gravity was measured through a 250 ml pycnometer filled with water and 50 g of 4.75 mm soil size at room temperature.

Geophysical investigations

The AMT survey measures natural electric field measurement and provides subsurface lithological characteristics and structural features, crucial for understanding groundwater accumulation and potential geological hazards, especially in hilly terrains (Aizawa

et al. 2009; Huang et al. 2021; Mekkawi et al. 2022; Xu et al. 2020). The application of the AMT model in the Domeshi Landslide has yielded valuable insights into the geological structures and dynamics underlying the event. By leveraging the AMT method, we have been able to enhance our understanding of known fault, such as the JF, and gain deeper insights into their subsurface immersion. These results will significantly contribute to our knowledge of the subsurface geological structures prevalent in the area affected by the landslide. Two geophysical profiles (Profile DD' and EE'; Fig. 4) were conducted along the landslide while one profile was conducted across the landslide (CC'). PQWT TC-500 instrument with an accuracy of 0.001 mV having 8 measurement channels was used in the field.

Petrographic examination

For petrographic examination, three rock samples from quartzite and 2 rock samples from dolomitic limestone were collected. Thin sections were prepared, and a polarized Leica DM 750 HD digital microscope was used for the microtextural and mineralogical investigations.

Kinematic study

The discontinuities within highly fractured rock masses can predispose slopes to circular or non-circular failures, as documented in previous studies (Hoek and Bray 1981; Mukherjee and Tayabe 2019). To assess the impact of these structural features on the stability of the Domeshi Landslide and anticipate potential failure mechanisms, a kinematic analysis of structural discontinuities was conducted. Field surveys on two sites (Fig. 4) were conducted to gather data on the orientations of slope-facing directions and the inclination of various discontinuity sets within the landslide area. The kinematic analyses were performed using Dips Version 7.0 software of rocscience by employing a stereographic projection technique that helps to determine the modes of failure. Hoek (2005) and Kliche (1999) worked on the kinematics and proposed some conditions for evaluating the planar mode of failure: (a) the failure plane must strike parallel to the slope face (i.e. $\pm 20^\circ$); (b) the plane of failure should be daylight in the slope face, i.e., the dip of the slope should be steeper than the apparent failure plane dip; and (c) the failure plane dip should be greater than plane's friction angle. When two or more discontinuities intersect at one point, the wedge mode of failure is likely to happen. Generally, in the wedge failure, the trend of intersection lines should be within 90° of the dip, whereas the plunge of the line should be daylight along the slope face which reveals that the slope dip is greater than the plunge of the line of intersection (Hoek 2005; Wyllie and Mah 2004).

Numerical modeling

Geotechnical parameters such as soil properties, shear strength, and groundwater conditions were determined through laboratory as well as in-situ testing to provide input for numerical modeling. Three main approaches were employed: FDM using FLAC and LEM using Slope/W and FEM using RS2 software. FLAC, based on finite difference theory, was utilized for FDM analysis to simulate the

behavior of the slope under various loading and boundary conditions. Material properties obtained from laboratory testing were assigned to zones within the FLAC model, and the model was subjected to gravitational and external forces to assess slope stability. Iterative analyses were conducted to determine the critical failure surface and calculate the FoS for the Domeshi Landslide. In parallel, Slope/W, based on LEM, was employed for stability analysis using a predefined failure surface approach. The slope was divided into discrete slices, and the equilibrium of forces acting on each slice was evaluated to determine the FoS against failure. Various methods, such as Bishop, Janbu, Spencer, and Morgenstern-Price, were applied within Slope/W to calculate the FoS for different slope geometries and soil conditions. Strength reduction FEM plane strain analysis has been used with metric units and Gaussian elimination solver. The maximum iteration is 500 for stress analysis with a tolerance of 0.001. The Mohr-Coulomb criterion is employed to define the (intact) rock and soil strength characteristics. Modeling is done in gravity loading with discretization of six-noded graded triangular finite elements. Slope stability models have been computed by FEM models before and after the landslide. The results from FLAC, Slope/W and RS2 analyses were compared and validated against field observations to assess the stability of the Domeshi Landslide and identify critical failure mechanisms.

Results and discussion

Field observations and landslide mapping

The Domeshi landslide, triggered after the rainy season of July 2023, represents a progressive catastrophic event that unfolded over several days. The landslide's progression from its initial phase on August 1, 2023, to complete failure on August 4, 2023, caused widespread devastation across the affected area (Fig. 6g, h; Supplementary Fig. S1). Dozens of residential buildings, paved road, agricultural land, and trees were lost and posed significant challenges for the affected community (Fig. 6). The observation of various cracks in nearby houses provides further evidence of the widespread impact of the Domeshi Landslide on the surrounding infrastructure and communities (Fig. 6a, i). These cracks serve as visible indicators of the significant ground movement and deformation associated with the landslide event.

The landslide exhibited a NW to SE direction, with the Jhelum River flowing from the toe of the landslide (Fig. 1c). Both the failure face and rocks dip towards the SE direction (Fig. 4). The landslide extended over a total length of 500 m, with the width varying from 218 m along the road to approximately 100 m in the toe area (Fig. 7). The detailed field observations indicate a complex type failure with three distinct movement types: (a) translational movement from main scarp to the about 150 m downslope, occurring within rock units of dolomitic limestone and quartzite (Fig. 6c); (b) rotational movement from 150 to 300 m, largely occurring within the clays of Murree Formation; (c) flow type movement below 300 m down to the riverbank (Fig. 7a). Numerous cracks, some spanning several meters, were observed within the landslide area (Fig. 6e, i). Additionally, springs and seepages were noted, suggesting groundwater influence in landslide dynamics (Fig. 6d). The presence of the active JF traversing the landslide body was identified, indicating potential tectonic activity contributing to slope instability (Fig. 6b). The JF was visibly delineated between the Murree Formation and Hazara

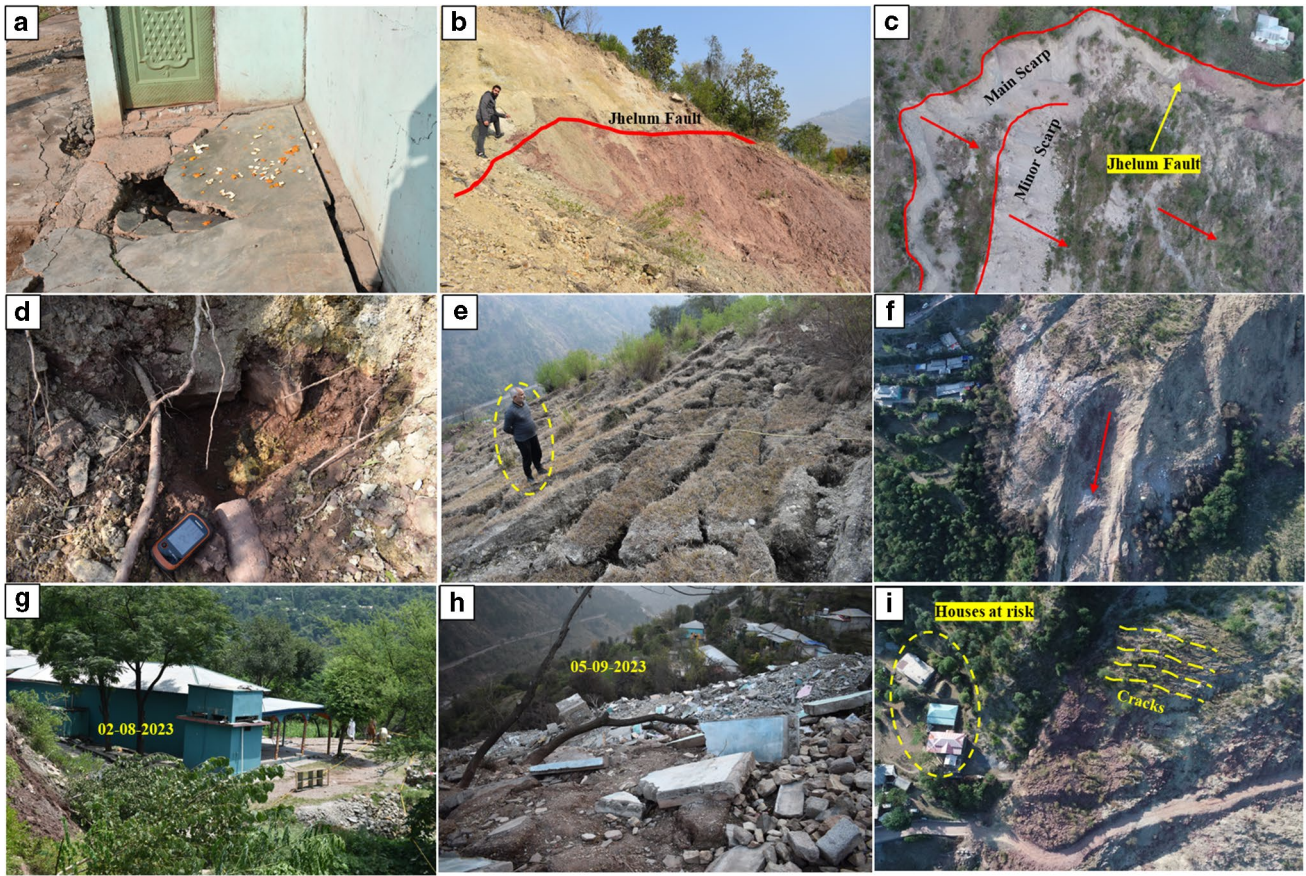


Fig. 6 Landslide features (location of photographs are shown in Fig. 1) observed in the field: **a** Cracks in the house adjacent to the left flank of landslide. **b** Jhelum Fault is clearly seen between maroon clays of Murree Formation and brecciated quartzite of Hazara Formation. **c** Landslide scarp and fresh exposure of dolomitic limestone. **d** New spring originated after landslide within the landslide body. **e** Multiple cracks were observed in the landslide body; yellow circle is for scale. **f** Flow like movement in the lower part of the landslide. **g** Condition of building in the 1st phase of landslide on 02-08-2023. **h** Complete collapse of the same building in the 2nd phase of landslide at 04-08-2023. **i** Right flank of the landslide: multiple cracks can be clearly seen; encircled houses have multiple fractures in the walls and basement and are at risk

Formation along the flanks of the landslide. Brecciated and gouged materials were observed along the fault plane, indicating past fault activity. Murree Formation clays, characterized by their maroon color and high plasticity, were prominently exposed on the landslide (Fig. 6f). The estimated slip surface of the landslide varied, reaching up to 25 m in certain sections.

The Domeshi Landslide exhibits varying slope angles along its profile, contributing to its dynamic behavior and susceptibility to failure (Fig. 7a). With a total height of 240 m, the slope angle varies significantly across different sections of the landslide. The slope angle exceeds 60° in the topmost part of the landslide, indicating steep terrain and heightened instability (Fig. 7a). The slope angle reduces to approximately 25–30° at the middle part of the landslide, reflecting relatively gentler terrain (Fig. 7a). However, at the lower part of the landslide, the slope angle increases sharply to around 55°, indicating a return to steeper terrain and potentially increased susceptibility to sliding (Fig. 6f; 7a). The average slope angle of the entire landslide is calculated to be more than 45°, highlighting the overall steepness of the slope and its predisposition to mass movement. Such steep slopes are inherently prone to instability, especially when combined with factors such as geological weaknesses,

intense rainfall, and tectonic activity (Soeters and Van Westen 1996). The variation in slope angles within the landslide suggests a complex failure mechanism involving multiple factors, including topographic variations, material properties, and structural controls. Historical Google Earth imagery depicted minor fractures and scarps preceding the complete failure, with subsequent images revealing the widening of fractures post-2021, likely influenced by seismic events and intensified rainfall due to climatic conditions (Supplementary Fig. S2).

Geophysical analysis

The AMT survey depicts the subsurface image of rocks and their structures by inferring the total variations in their electric and magnetic fields (Khan et al. 2024). A total of three AMT profiles were acquired. The NNE-SSW profile C–C' (Fig. 4) reveals the distribution of unconsolidated material, primarily clays of the Murree Formation, up to a depth of 30 m (Fig. 8). There are no discernible horizontal or vertical discontinuities observed within this depth range. Beyond 30 m, hard and intact rocks, such as sandstone of the Murree Formation, dominate the subsurface,

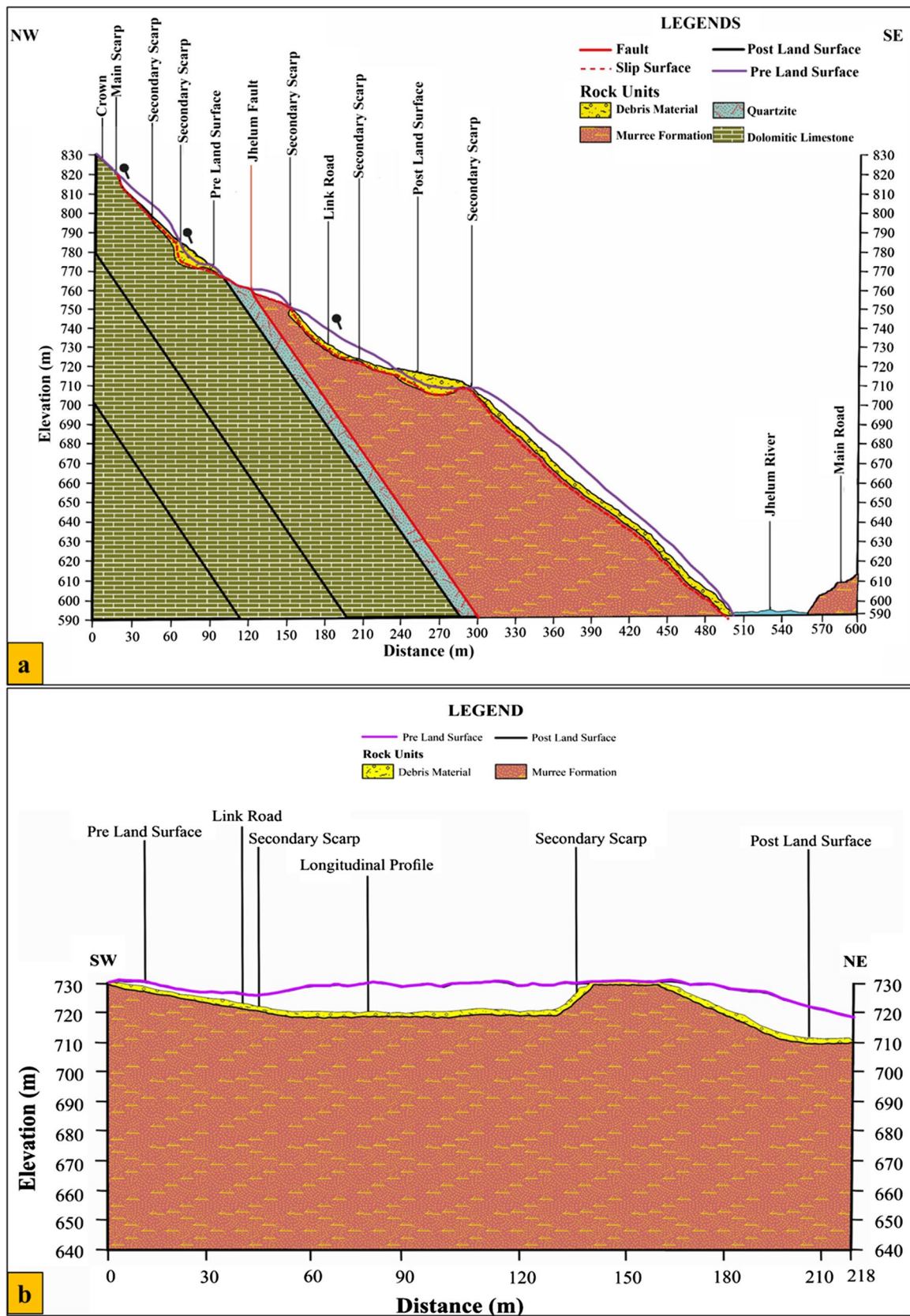


Fig. 7 a Longitudinal NW-SE oriented A-A' profile. b Cross SW-NE oriented B-B' profile of the landslide (as shown in Fig. 4)

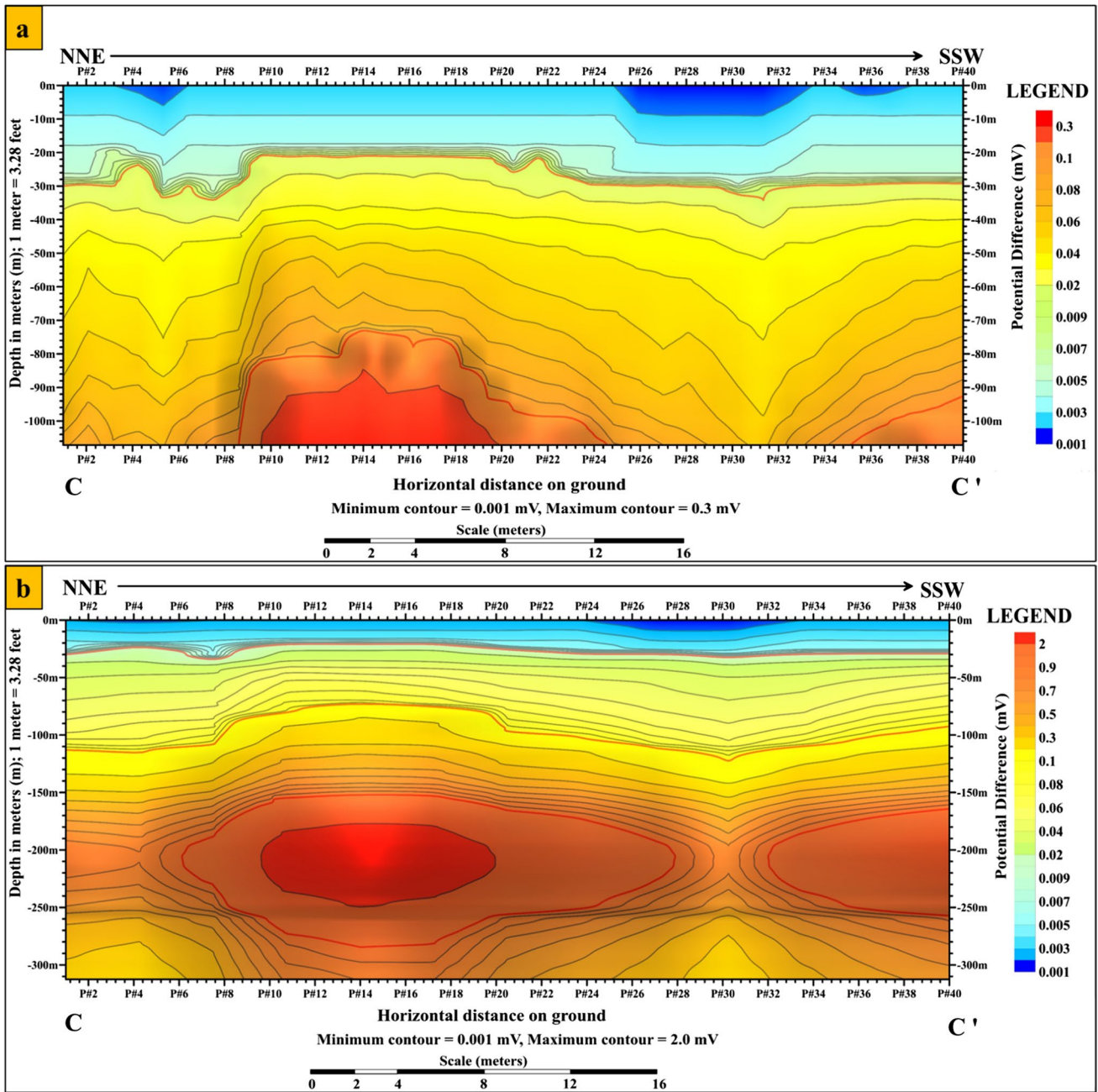


Fig. 8 Geophysical survey profiles (location of profile can be seen in Fig. 4). **a** Iso-anomaly contour map of AMT data (Profile 1: C–C') up to the depth of 107 m. **b** Iso-anomaly contour map of AMT data (Profile 1: C–C') up to the depth of 312 m

extending to a depth of 107 m (Fig. 8a). Notably, the absence of significant fractures or discontinuities up to a depth of 150 m suggests relative stability within this portion of the subsurface. The distribution of the electric field of rocks from the surface to the depth of 312 m along profile C–C' is shown in Fig. 8b. In SE–NW profile D–D' (Fig. 4), the distribution of the electric field indicates the presence of unconsolidated material from the surface to a depth of 25 m, with electric field values ranging from 0.001 to 0.01 mV. Beyond 25 m, hard and intact rocks dominate, extending to a depth of 107 m indicating the presence of

consolidated strata within this depth range. These rocks likely exhibit higher electrical resistivity compared to the surrounding materials, reflecting their consolidated and impermeable nature. Several fractures were observed at points 12, 16, 38, and 54, exhibiting varying depths and are likely indicative of structural weaknesses within the subsurface (Fig. 9a). These fractures were also observed on surface during the field. Figure 9b illustrates the distribution of electric field values from the shallow surface to a depth of 312 m along profile D–D'. The electric field values range from 0.001 to 0.9 mV across the profile, indicating

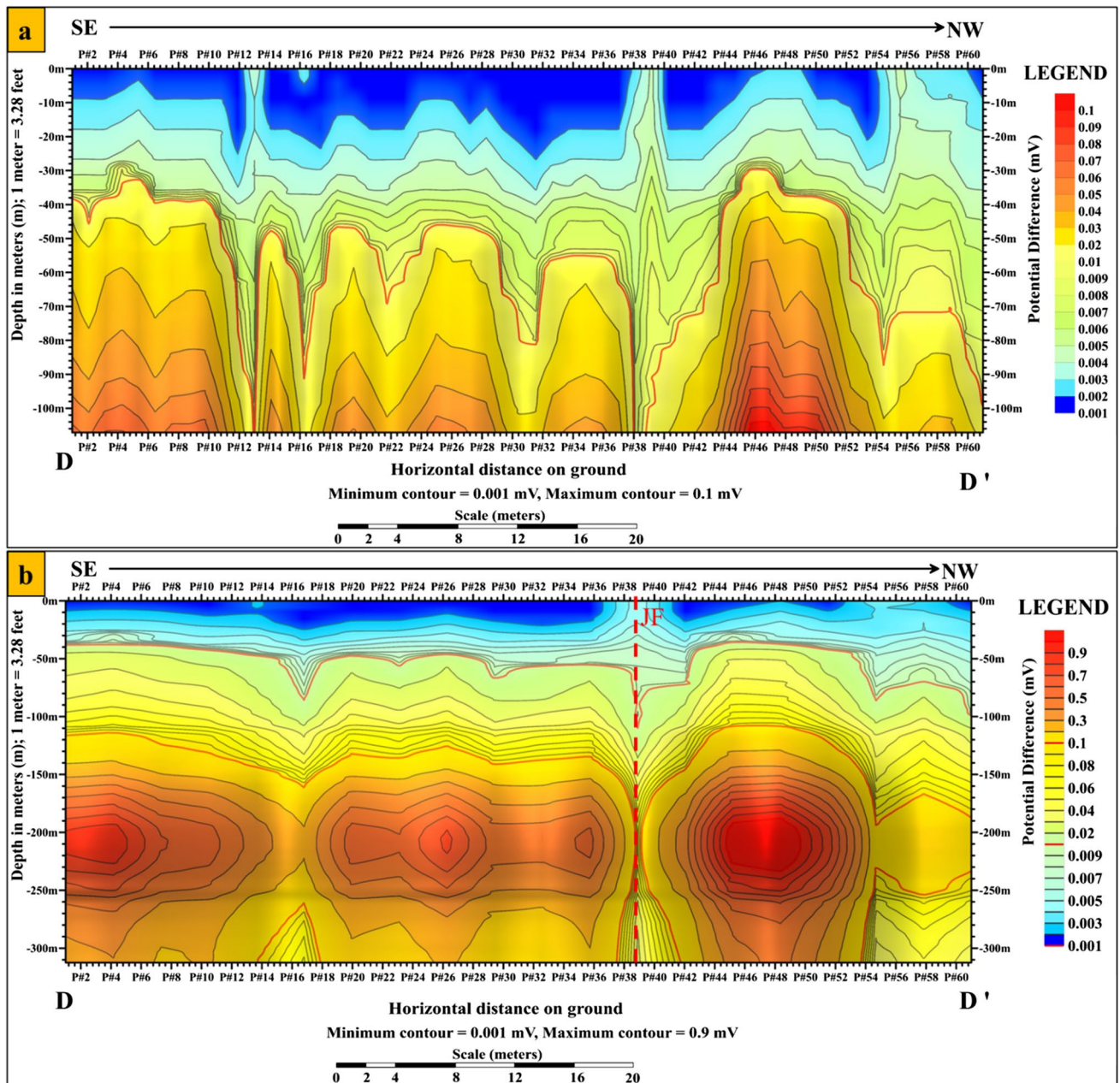


Fig. 9 Geophysical survey profiles (location of profile can be seen in Fig. 4). **a** Iso-anomaly contour map of AMT data (Profile 2: D-D') up to the depth of 107 m. **b** Iso-anomaly contour map of AMT data (Profile 2: D-D') up to the depth of 312 m

variations in subsurface lithological properties and structural features. Notably, a deep fracture is observed at point 38, located 79 m from the initial marked point on the ground surface. This fracture extends beyond a depth of 300 m and is hypothesized to coincide with the JF, given its proximity to the fault line (Fig. 9b). Fractures associated with major fault lines like the JF can serve as conduits for groundwater flow and may influence the stability of surrounding geological formations. The NW–SE profile E-E' (Fig. 4) further highlights the presence of vertical fractures at specific points, such as points 6 and 31, extending up to a depth

of 250 m (Fig. 10). Additionally, profile E-E' depicts hard rocks distributed from 130 to 250 m in the subsurface, suggesting the presence of stable geological formations within this depth range. Figure 10a shows the distribution of the electric field of rocks from a shallow surface to the depth of 107 m along profile E-E'. The electric field ranges from 0.001 to 0.04 mV throughout the profile. The vertical fractures are present at point 6 (which is 15 m on the ground from the initial point) and point 31 (which is 65 m on the ground from the initial marked point) up to a depth of 250 m in the subsurface (Fig. 10).

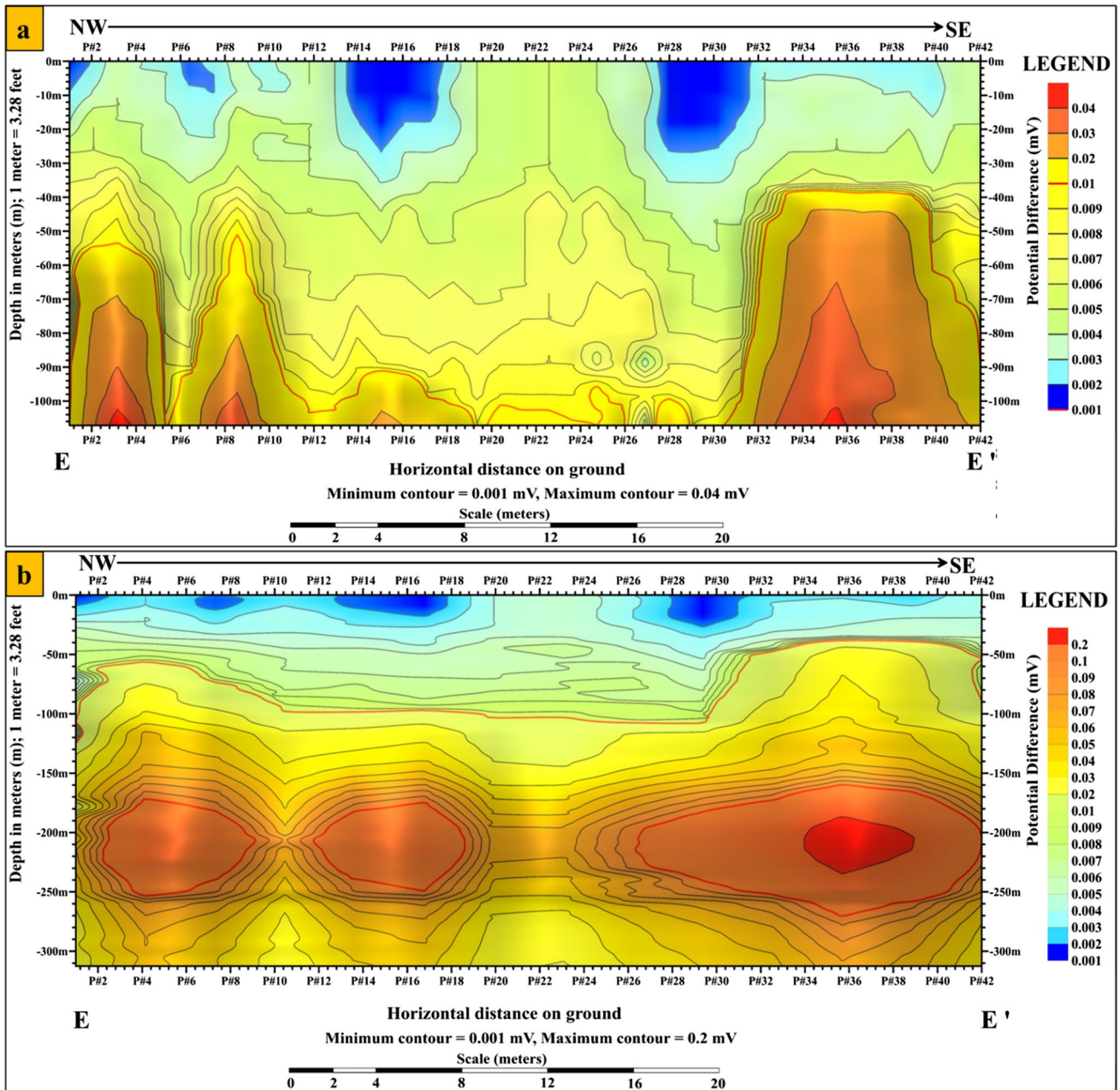


Fig. 10 Geophysical survey profiles (location of profile can be seen in Fig. 4). **a** Iso-anomaly contour map of AMT data (Profile 3: E-E') up to the depth of 107 m. **b** Iso-anomaly contour map of AMT data (Profile 3: E-E') up to the depth of 312 m

Overall, the AMT results provide valuable insights into the subsurface lithological variations and structural characteristics, aiding in the assessment of potential slip surface and structural discontinuities. The results indicate that Domeshi Landside is a fault-controlled landslide, characterized by unconsolidated material on the top layer along with several deep fractures destabilizing the slope and making it prone to failure after heavy rainfall. These findings are comparable with the findings of Wang et al. (2022) that investigated the 2021 fault-controlled Chengtian landslide in China triggered by rainfall.

Geotechnical experimentation

The grain size distribution has a significant impact on landslide occurrence and movement (Yalcin 2011). The mechanical sieve analysis provides the soil grain structure along with its size, shape, and distribution, whereas the packing of grains holds the soil structure. Three major soil fractions, i.e., fines (silt and clays), sands, and gravels (non-cohesive), have been observed through grain size distribution analysis in the soil samples from Domeshi Landslide (Fig. 11a). The grain shape analysis shows a variation of angular to rounded particles in varying proportions throughout the

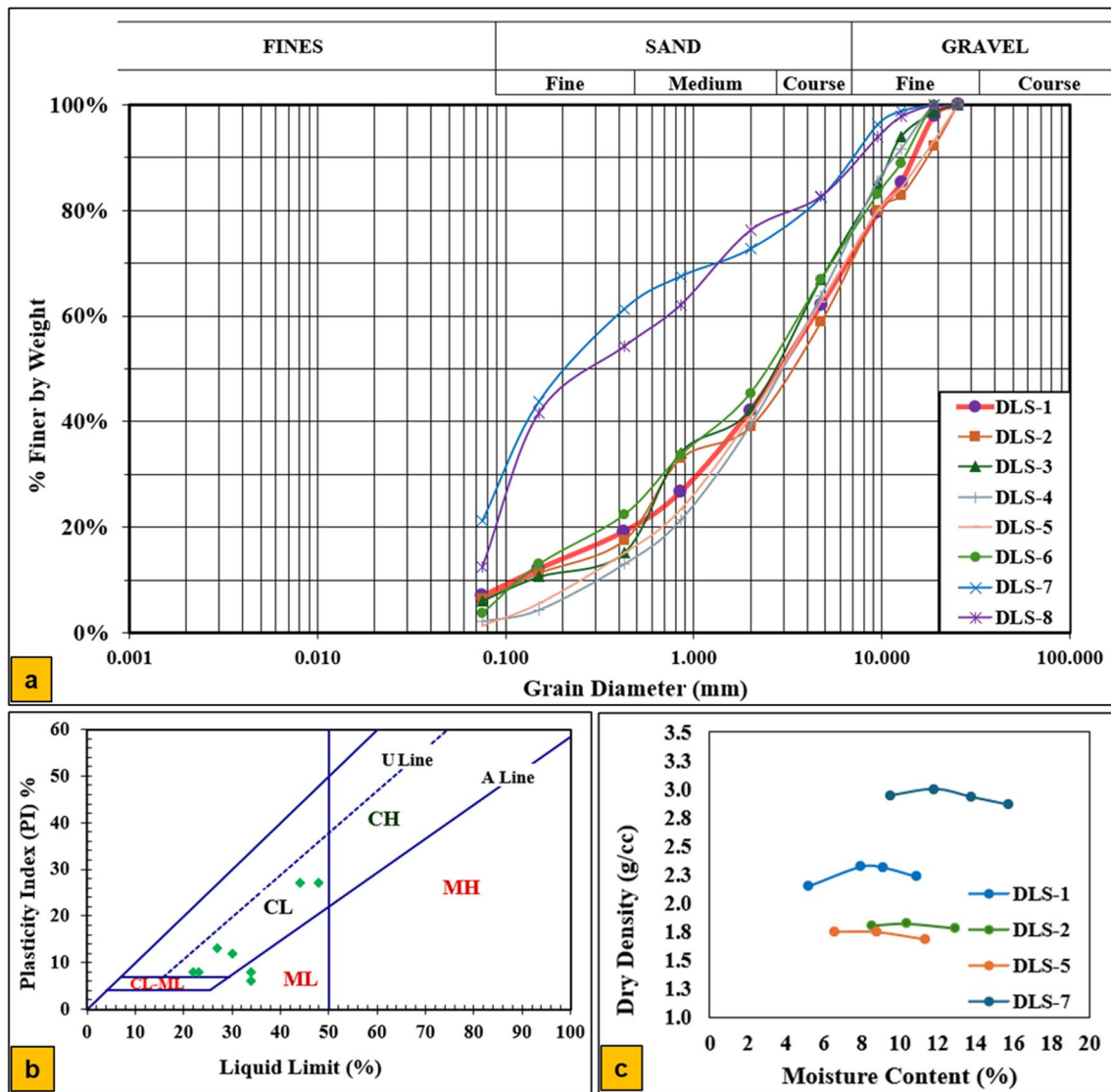


Fig. 11 Engineering properties of the soil samples from Domesi Landslide. **a** Grain size distribution analysis. **b** Casagrande plasticity chart. **c** Moisture-density relationship

landslide body. The results indicate an overall dominance of sand fraction while the clay fraction dominates the samples along the fault zone (Fig. 11a). The dominance of the sand fraction supports the higher infiltration through the slope material thereby causing an increase in pore water pressure. These results are in line with Khan et al. (2021) who investigated the rainfall-triggered Danna-Sahotar Landslide in the southeast of Muzaffarabad. According to Mukasa-Tebandeke et al. (2015), soils with a higher content of clays expand during wetting and drying conditions. The dominance of clay fractions along the fault is aligned with the results of Kitutu et al. (2009) who worked on the slope of Mount Elgon and concluded that landslide occurrence is due to the abundance of clay size materials along the slopes. Moreover, the present study is consistent with other studies concluding that the higher clay content greatly influences landslide triggering (Wang et al. 2020; Mugagga et al. 2012; Knapen, et al. 2006; Wati et al. 2010).

The moisture content determination is a key indicator to evaluate the soil engineering properties and their behavior to determine its deformation or failure criteria specifically for slopes containing soil material (Ma et al. 2023). The transitions from solid to semi-solid and then to plastic state reveal that the failure planes consist of soils that may contribute to the landslide-triggering mechanism during heavy rainfalls (Askarinejad et al. 2018). The values of natural moisture content range from 14.4 to 18.7%, LL ranges from 22 to 48%, PL ranges from 14 to 28%, while PI ranges from 6 to 27. The results indicate that most of the samples possess zero shrink-swell potential except the soil samples DLS-7 and DLS-8 which possess higher PI (Table 1). The soil samples DLS-1 to DLS-6 are non-plastic to low-plastic soils, therefore these soils are inelastic which suggests that these soils would not regain their total initial volume while loading (Table 1; Fig. 11b). In contrast to the findings of Khan et al. (2021), the soils in the Domesi Landslide are more plastic,

Table 1 Engineering properties of soil samples of Domeshi landslide

Sample ID	In-situ bulk density g/cm ³	Moisture content %	Specific gravity	LL %	PL%	PI %	OMC %	MDD g/cc	Cohesion kPa	Angle of Internal friction ϕ	USCS
DLS-1	1.942	14.4	1.55	34	26	8	8.4	2.4	15.78	19.96	CL
DLS-2	1.408	15.7	1.62	30	18	12	9.1	1.8	CL
DLS-3	1.47	22	14	8	ML
DLS-4	1.44	23	15	8	ML
DLS-5	1.393	15.4	1.65	34	28	6	10.8	1.78	11.84	20.88	ML—CL
DLS-6	1.64	27	14	13	CL
DLS-7	2.547	18.7	1.79	48	21	27	11.9	2.99	16.4	18.00	CL—CH
DLS-8	1.77	44	17	27	CL—CH

specifically along the fault line. Moreover, this analysis also indicates that the excessive moisture content along with other factors can interfere with the consistency behaviors. The analysis has led to considering the PI as an influential parameter with respect to the soil water retention properties and swelling characteristics along the slip surface (El Jazouli et al. 2022). It is significant, however, that the slope failure in the study area corresponds to the monsoon rainfall distribution during July 2023 (Fig. 2b).

The moisture density relationship of the soils is obtained through the Proctor test which indicates the degree of compaction for varying sized soil particles. Results of the Proctor test show the values of OMC vary from 8.4 to 11.9% and MDD varies from 1.8 to 2.99 g/cc (Table 1; Fig. 11c). The results indicate that the loose soils possess porous structures in the natural state; therefore, these soils are compressible. The varying size soils can be compacted to enhance their engineering characteristics and behavior under vibrations and loading. This compaction effort can be helpful to improve the soil's shear resistance, bearing capacity, and stability to enhance factor of safety and density of soil. Based on the test results, the soil samples DLS-1, DLS-2, and DLS-3 require maximum compaction effort as these soils are in a loose state, whereas DLS-7 requires less compaction efforts due to their cohesive nature (Fig. 11c; Table 1). The specific gravity is an index property which reflects the mineralogical composition and indicates the ratio of the void spaces of the soils (Oyediran and Durojaiye 2011). The specific gravity values of all the samples collected range from 1.44 to 1.79, with an average value of 1.61 (Table 1).

The shear parameters, i.e., cohesion and angle of internal friction show the ultimate resistance to the applied stress. The cohesion and angle of internal friction values range from 11.84 to 16.40 kPa and from 18° to 20.88° respectively (Table 1). Higher friction angles indicate the relatively sandy soils while higher cohesion represents the clayey soils. The minimum cohesion values of the soil samples can be considered as the critical equilibrium state throughout the slope materials except for the soil samples collected from the fault zone. This implies that the failure occurs when the slope material is saturated. Moreover, the shear parameters analysis revealed that low angle of internal friction values possess high vulnerability to

slope failure. The results of the direct shear test on rock samples are presented in Table 2. The average values of frictional angle, cohesion, and unit weight of dolomitic limestone are 74°, 215 kPa, and 28.06 kN/m³ while those of quartzite are 38.59°, 350 kPa, and 29.74 kN/m³ respectively. The influence of stresses in context with the mode of failure is calculated through these tests. Moreover, shear parameters were also drawn to verify the slope stability analysis of this slide. The rock samples were tested under varying confining pressures. The degree of fracturing initiated during the test can also be a critical parameter to characterize the impacts of confining pressures, i.e., crack density is inversely proportional to the applied confining pressures (Li et al. 2017). Various components influence the shear parameters of the rock discontinuities which include joint size, aperture, strength, weathering, in-situ stresses, and filling material (Barton and Choubey 1977; Liu et al. 2017).

In the quartzite rock samples, the cracks were observed nearly parallel to the specimen axis depicting a brittle behavior which splits the quartzite sample along the pre-defined quartz veins (Fig. 12 sample A, B). The shear and varied modes of failure were observed in the dolomitic limestone as these samples exhibited traces of tensional cracks which represent that dolomitic limestone is influenced by the combination of tension and shear deformation against the confining pressures of 0 to 10 MPa and 15 MPa (Fig. 12 sample C, D). Moreover, the post-depositional features like microfractures (Fig. 12a sample C), can be seen in the sample before testing and major failure planes following these attributes can be observed after testing the sample (Fig. 12b sample C).

Petrographic analysis

Two rock units namely quartzite and dolomitic limestone exposed at the Domeshi Landslide have been studied for petrographic characteristics. Petrographically, the quartzite mainly comprises of quartz (> 97%) with minor feldspar followed by mica and traces of tourmaline. The quartz grains are medium to coarse-grained, mainly elongated, occasionally subangular to surrounded, undulatory and non-undulatory. The quartz grains mainly show the suturing, concavo-convex and planar

Table 2 Mohr–Coulomb constitutive model properties of Domeshi Landslide obtained through laboratory and in-situ tests using for slope stability analysis

Lithological units with intact and slide conditions	Slope stability model parameters								
	Unit weight (KN/m ³)	Peak cohesion (kPa)	Peak angle of friction (°)	Peak tensile strength (MPa)	Residual cohesion (kPa)	Residual angle of friction (°)	Young's modulus (MPa)	Poisson's ratio	
Intact	Clays	17.3	17	19	0.0036	12.75	15.2	22	0.27
	Dolomitic limestone	28.064	215	74	3.75	161.25	59.2	63	0.26
	Quartzite	29.748	350	38.59	5.38	262.5	30.82	72	0.12
Landslide portion	Clays	15.5	15.80	24	0.0028	11.85	19.2	17	0.21
	Dolomitic limestone	27.973	208	77	3.20	156	61.6	56	0.23
	Quartzite	28.575	342	41.20	5.15	256.5	32.96	68	0.10

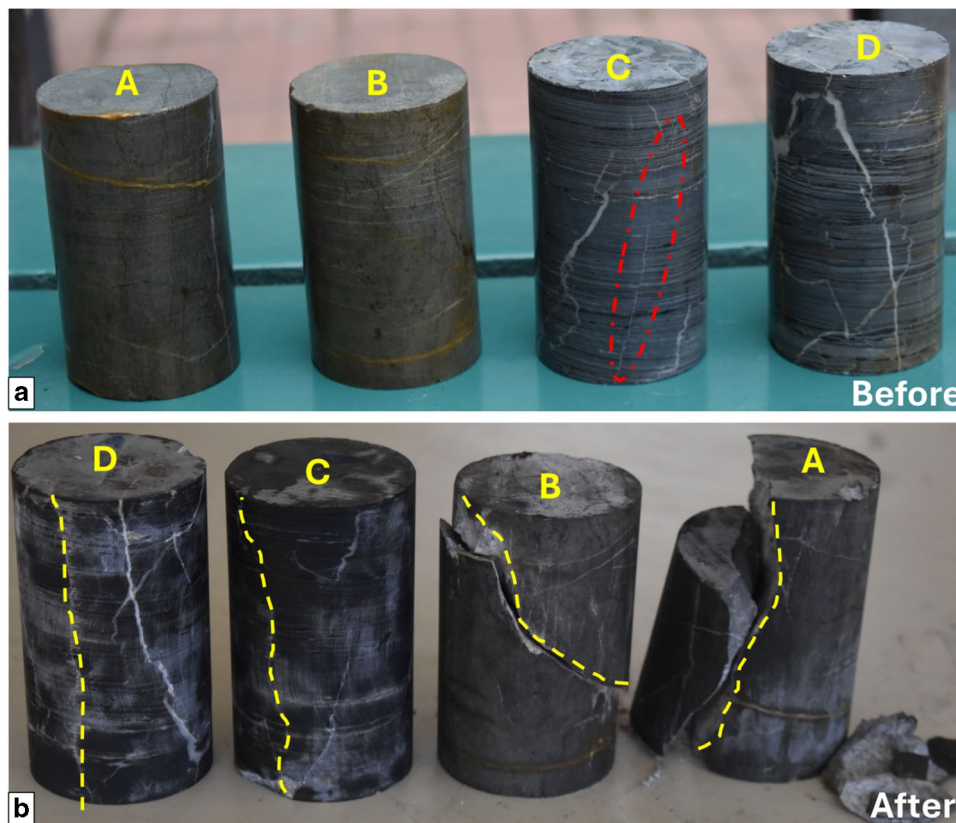


Fig. 12 Examples of common failure modes observed in (A-B) hard brittle quartzite and (C-D) dolomitic limestone under triaxial compression (a) before and (b) after testing photographs (core specimens are ~54 mm in diameter); (A) Brittle failure along a pre-existing discontinuity in quartzite unit (B) Brittle shear failure along the intact rock and pre-existing discontinuities in quartzite unit; (C) Intact-axial failure in dolomitic limestone; (D) Axial mode of failure along pre-existing discontinuities and intact rock in dolomitic limestone

contacts among the grains. Diagenetic features like pressure solution seams, i.e., stylolites, and open and microcrystalline quartz-filled fractures were common while occasionally

chlorite matrix-filled intergranular spaces were also observed. Intergranular and intragranular tectonic fractures were also observed which show intense deformation (Fig. 13d–i). The

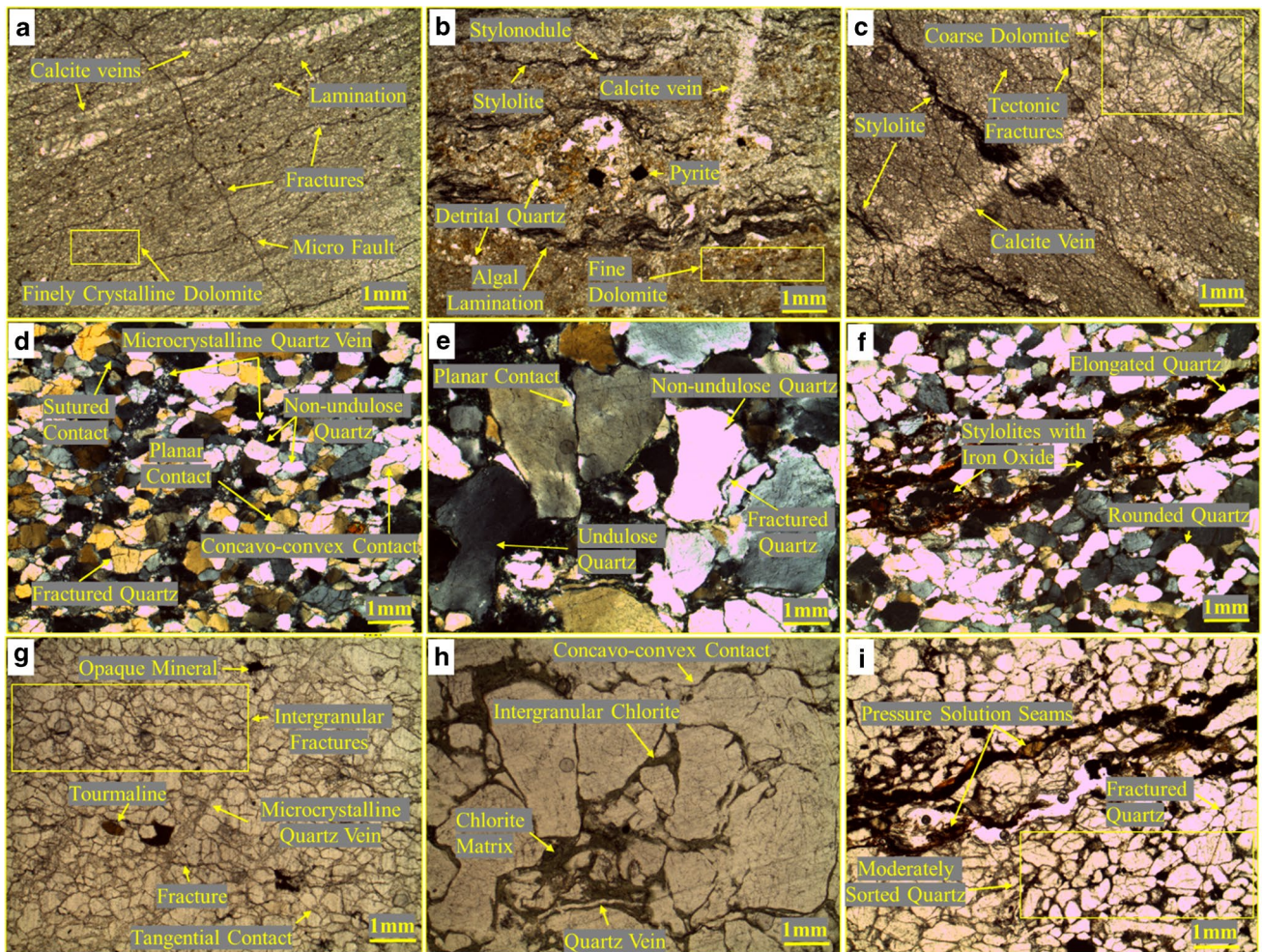


Fig. 13 Photomicrograph showing **a** finely crystalline dolomite with multiple sets of fractures and calcite veins; **b** algal laminated dolomitic limestone with stylolites, scattered quartz, and pyrite; **c** dolomite with cross cutting stylolites and calcite filled fractures; **d** medium grained quartzite with non-undulose and undulose quartz; **e** coarse grained quartzite with undulose quartz grains having different intergranular contacts; **f** quartzite with elongated quartz grains and tectonic stylolite seams; **g** quartzite with inter and intra-granular fractures; **h** quartzite with chlorite scattered within intra-granular quartz grains; **i** moderately sorted quartz with pressure solution seams (**a-i** 4X; **a-f** XL, **g-i** PPL)

dolomitic limestone dominantly consists of micrite (95%) with minor microcrystalline dolomite scattered on the micrite matrix. The dolomite mainly consists of dolomite interlayered with limestone and the occasional presence of detrital quartz grains on a centimeter to millimeter scale. The dolomite is fine-grained with subhedral dolomite crystals, and minor diagenetic pyrite with horizontal to wavy thinly laminated algal mates. Diagenetic features like stylolites and calcite-filled fractures were observed in cross-cutting relationships. The rock unit is devoid of any fossils (Fig. 13a–c). The textural and microstructural properties in quartzites can reveal various deformation processes and conditions responsible for their formation (Wilson et al. 2022). According to Stipp et al. (2010), quartz grains can be recrystallized to larger sizes with an increase in temperature and a decrease in strain rate. Hence, this phenomenon can be used to determine the paleo-stresses responsible for the natural deformation of rocks (Behr and Platt 2011). The undulatory quartz is also an indication of superplasticity resulting in deformation bands and lamellae

under intense stresses (Blenkinsop 2007). Similarly, the behavior of carbonate rocks under natural stresses has important implications for dynamic processes of fault zone formation and slope stability (Lisabeth and Zhu 2015; Li et al. 2018).

The primary and secondary structures in studied carbonates such as fractures, calcite-filled veins, and stylolites are considered to reduce the strength of rock units against prevailing stresses. The primary (depositional) and secondary (tectonic) inter- and intra-granular fractures, stylolites, and mineralogical alterations indicate that the rock formations are subjected to intense deformation. This understandably correlates with the megascopic features as well as the tectonic and structural settings of the area (Srivastava et al. 2016). These rock units are exposed along the JF running through the head of the Domeshi Landslide under discussion. Hence, it can be concluded that the active deformation along this fault has considerably reduced the strength and durability of rock units and made them vulnerable to failure under coupled geological and hydrometeorological factors.

Kinematic analysis

In the current study, the kinematic analyses were performed on the discontinuity data collected from the two sites (Fig. 4). The rock mass is highly jointed and sheared with various joint sets found along the scarp. The planar and wedge failure modes of the rocks along the landslide scarp are common due to the steeply dipping discontinuities (Fig. 14). Moreover, the discontinuities mostly dip parallel to the slope face; therefore, the planar mode of failure is mostly abundant along this landslide (Fig. 14a–c). The J_1 joint set is mainly responsible for the planar failure along this slope, whereas J_1 and J_R intersections contributed to the wedge failures at site 1 (Fig. 14a, b); whereas

at site 2, J_1 and J_R are responsible for the planar failure while the intersection of J_1 and J_2 as well as J_2 and J_{R2} are posing threat to the wedge failure along the scarp of the Domeshi Landslide (Fig. 14c, d). The current results align with the findings of Hamasur, (2022) who worked on the kinematic analysis and Q-slope assessment of rock slopes in Iraq and concluded that planar and wedge-type modes of failures are mainly responsible for the slope failures. According to Sharma et al. (2019), discontinuity patterns strongly influence the rock slope instability along the road cuts. Hence, it can also be concluded that the discontinuities of rock units exposed along the scarp and on the flanks of the landslide are dipping towards the slope face, which has the potential of further slope failure.

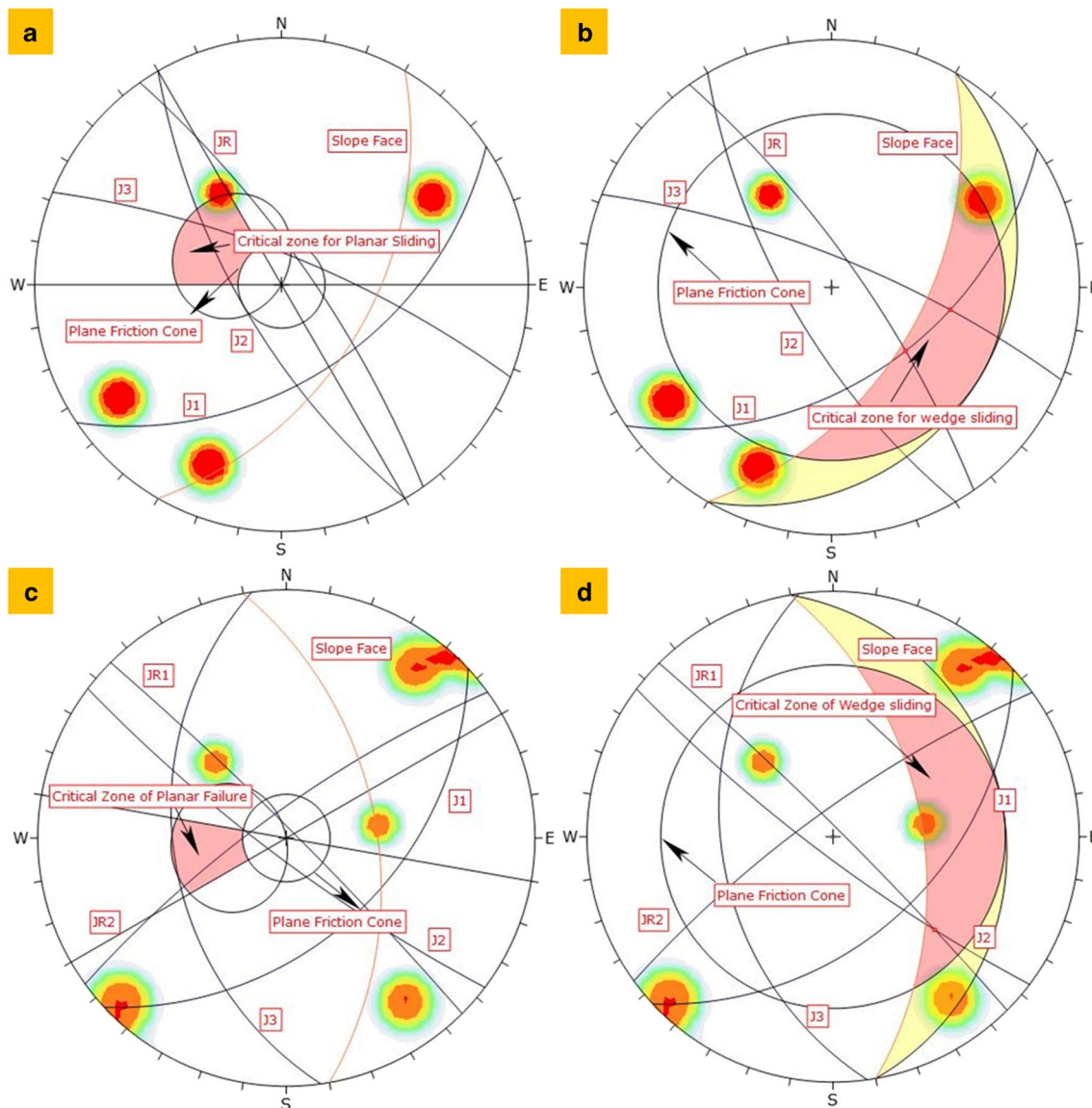


Fig. 14 Stereographic projections of the discontinuity data sets of Domeshi Landslide rock units exposed along the scarp. **a** Planar mode of failure along joint set 1 and **b** Wedge mode of failure along the intersection of joint sets 2 and random joint set (JR) and along the intersection of joint set 3 and random joint set (JR) **c** Planar mode of failure along joint set 1 as well as along random joint set (JR1) and **d** Wedge mode of failure along the intersection of joint sets 2 and random joint set (JR1) and along the intersection of joint set 1 and joint set 2

Slope stability analysis

The slope failures primarily occur due to increased shear stresses or decreased shear strength of the slope material. A comprehensive slope stability analysis therefore encompasses the evaluation of geological and geomorphological factors, material properties, and shear strength parameters. FEM, LEM, and FDM were employed for slope stability analysis at the Domeshi Landslide. The input parameters for slope stability analysis have been obtained via in-situ and laboratory experimentation and results are presented in Table 2. The boundary and geometry conditions were kept the same as those in Fig. 7a. FLAC uses mass density, whereas Slope/W uses unit weight in the material properties along with cohesion and angle of internal friction. The FoS for the Domeshi landslide calculated through FDM is 0.56, while through LEM including Ordinary, Bishop, Janbu, Spencer, and Morgenstern-Price methods are 0.811, 0.838, 0.810, 0.837, and 0.88, respectively (Fig. 15; Table 3). The comparative analysis of FoS and SRF depict that FoS is less than 1 which suggests that the slope is unstable (Table 3). Variation in the FoS indicates that the FLAC slope provides minimum FoS (0.56;

Fig. 15f) as compared to LEM because the material deformation is considered in FLAC numerical simulation but not in LEM. These results are in accordance with Soren et al. (2014) and Wang et al. (2013). Similarly, small variations in the FoS among the different LEM methods are in accordance with the study conducted by Khan et al. (2021). The critical slip surface is visible in all the employed methods which reveals that the lower part of the Domeshi Landslide has a potential for future failure.

Strength reduction FEM

Both pre and post landslide models are computed for Domeshi Landslide using SSR-based FEM (Figs. 16 and 17). The failure planes as determined by the RS2 program follow partly fault surfaces and partly pass through intact rock mass. The total displacement and the maximum shear strain contours provide a potential shear failure surface. The shear strain contours by Mohr–Coulomb criteria of each slope were shown in Figs. 16a and 17a. The critical SRF for pre-event and post event conditions are 1.15 and 0.44 respectively (Table 3). Failure surfaces are almost similar in shape when comparing with LEM and FDM analysis results (Figs. 15 and 17).

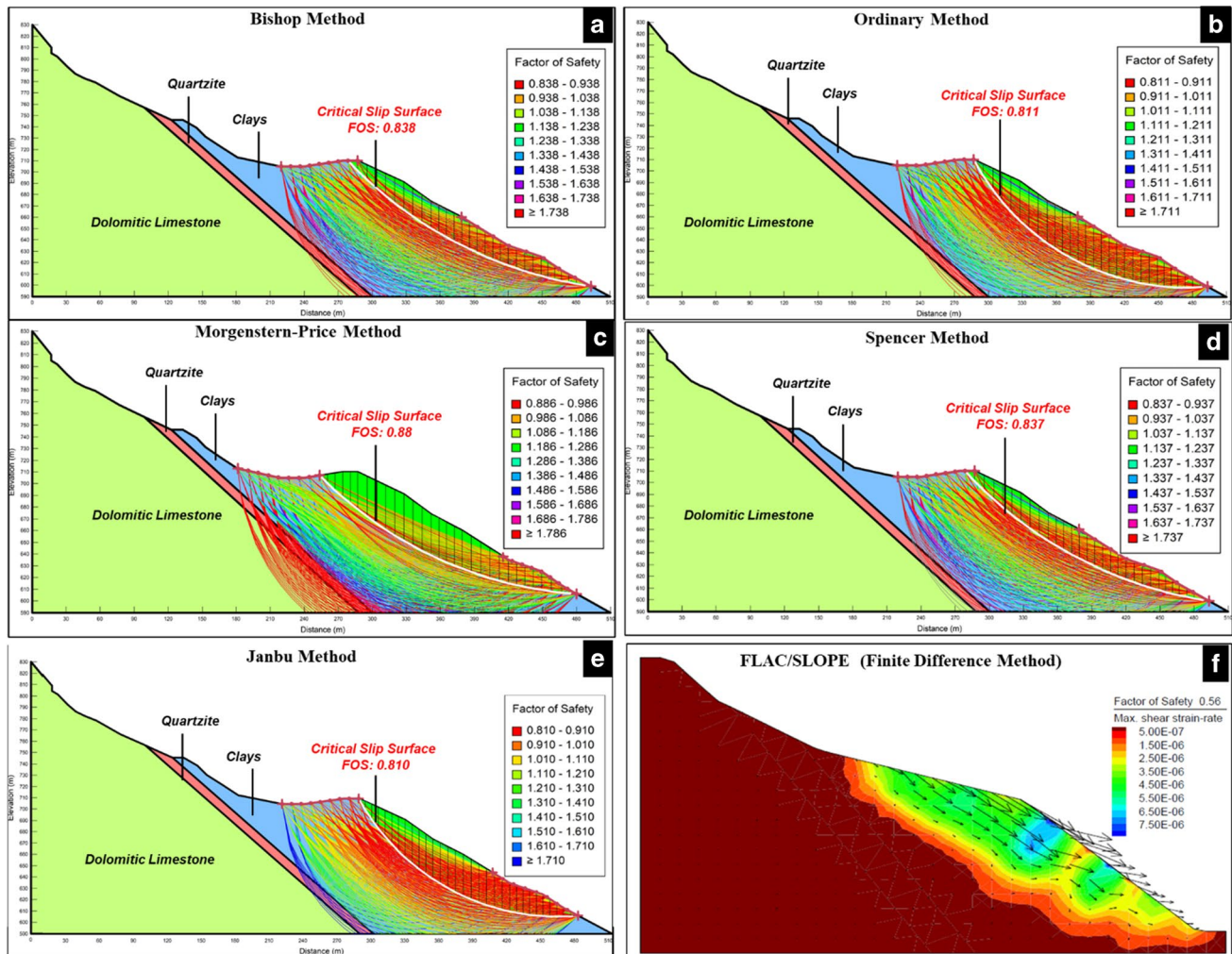


Fig. 15 Slope stability analysis using LEM in SLOPE/W software—FoS of Domeshi Landslide using **a** Bishop method, **b** Ordinary method, **c** Morgenstern-Price method, **d** Spencer method, **e** Janbu method, **f** FoS of Domeshi Landslide using FDM in FLAC software

Table 3 Comparison of FoS and SRF obtained through different methods

Landslide conditions	LEM FoS					FDM FoS	FEM	
	Ordinary method	Bishop method	Janbu method	Spencer method	Morgenstern-Price method		Critical SRF	Maximum total displacement (m)
Pre-event	–	–	–	–	–	–	1.15	2.22
Post-event	0.811	0.838	0.810	0.837	0.88	0.56	0.44	5.61

Furthermore, the total displacement of rock and soil can be derived from these input data with FEM. The critical failure surface and shear strain at the time of failure is illustrated in Figs. 16 and 17. Regions of high shear strain would represent the pathway where failure would most likely occur within such a modeled rock mass. The maximum shear strain on the critical failure surface for pre- and post-event is 0.458 and 2.85 respectively (Figs. 16a and 17a). The maximum total displacement in pre-event and post-event is found to be 2.22 m (Fig. 16b) and 5.61 m (Fig. 17b), respectively. It is observed that the failure surface and its location as estimated using numerical approach also matches with field observations (Fig. 7a). In the field, many tension cracks were observed indicating possible future slope failures. The analysis of pre-event result revealed SRF is > 1 in static conditions which failed after heavy rainfall in July 2023. Additionally, the geometry of the slope and orientation of fault likely has a greater role in destabilizing this area. The post-event model result also shows that the lower section of landslide remains unstable due to high slope angle with $SRF < 1$ (Fig. 17b). This is consistent with the results of FDM and LEM as well as field observations. The rock units exposed along the landslide site possess anisotropic behavior, therefore, the stress strain behavior is also varied. Along the scarp, the dolomitic limestone and quartzite are controlled mainly through the structural discontinuities especially along the parallel dip-slope and slope face orientations. Moreover, the presence of JF which runs across the landslide body also contributed to the failure mechanism and anisotropic behaviors of the slope material. The geomechanical and geotechnical parameters of the materials are also influenced by these structural elements in proximity. The strength results of rock units indicate that the quartzite units have medium to high strength while the dolomitic limestone indicates the low to medium strength along the rock slope. The highly plastic nature of clays leads to the reduction of shear strength when water infiltrates through these clays. This strength reduction is due to the increasing pore water pressure, soil suction, and increasing soil unit weight. Likewise, the shallow ground water table also contributed to the failure mechanism as two springs and a drainage along the right flank of the landslide were observed during field investigations. The rise in pore water pressure may initiate the stress reduction factor which lead to the failure of slope.

Failure mechanism of the landslide

The integrated analysis, numerical simulation, and field investigation led to a conceptual model for the landslide mechanism shown in Fig. 18. The activation and the failure of this landslide

took place in four stages which are in line with the investigations of Sun et al. (2022) who investigated the rainfall triggered landslide triggered in July 2016 in China. The pre-existing conditions of the Domeshi Landslide were initially identified by headscarves that resulted in cracks, many shown on historical Google Earth images (Supplementary Fig. S2). There was no sign of a landslide scarp in 2002. However, by 2009, a scarp and tension cracks had developed, likely due to a significant 7.6 Mw earthquake in 2005, with its epicenter located just 30 km northeast of the landslide site. This earthquake triggered numerous landslides in the region. Due to shaking of earthquake, the geological material gradually deformed, and a series of tension cracks formed on the crest of the slope. In the subsequent years, particularly noted in the 2010 image, some cultivation of the land began. Road construction inside the landslide body in 2019 also destabilized the slope. In the second stage, the main scarp is developed as shown in historic image of 2021 indicating the development of slip surface. This progression persisted into 2022 and 2023, as the main scarp deepened while cracks on its crest lengthened. There was an extreme rainfall of 420 mm in July 2023, which led to the development of cracks in buildings, roads, and the ground, resulting in the collapse of roads, buildings, and other infrastructure. This is the third stage of landslide failure mechanism. On August 1, the upper part of the landslide fully collapsed, while the lower part remained intact. This suggests that water percolation through fractures and fault planes led to an increased pore water pressure, ultimately causing the failure of the upper part. During the final stage (4th of August), the lower part of the landslide material moved like a flow due to the pushing effect of landslide material. Landslide triggering and causative factors are described in detail according to field investigation and deformation failure analyses as follows:

1. **Anthropogenic activities:** Human activities played a significant role in conditioning the landslide (Quevedo et al. 2023). Construction of buildings and road within the Domeshi Landslide disrupted natural drainage patterns and added weight to the slope. The drainage systems in the landslide area and springs allowed water infiltration to greater extent, which influenced negatively on slope stability. Additionally, agricultural activities, including cultivation, disturbed the soil and vegetation cover, reducing the slope's natural resistance to erosion and instability.
2. **Material heterogeneity:** The landslide site has three types of rocks including dolomitic limestone, quartzite, and clay. The strength and weathering of these rock units varied greatly. The 2005 Kashmir earthquake significantly weakened these rocks,

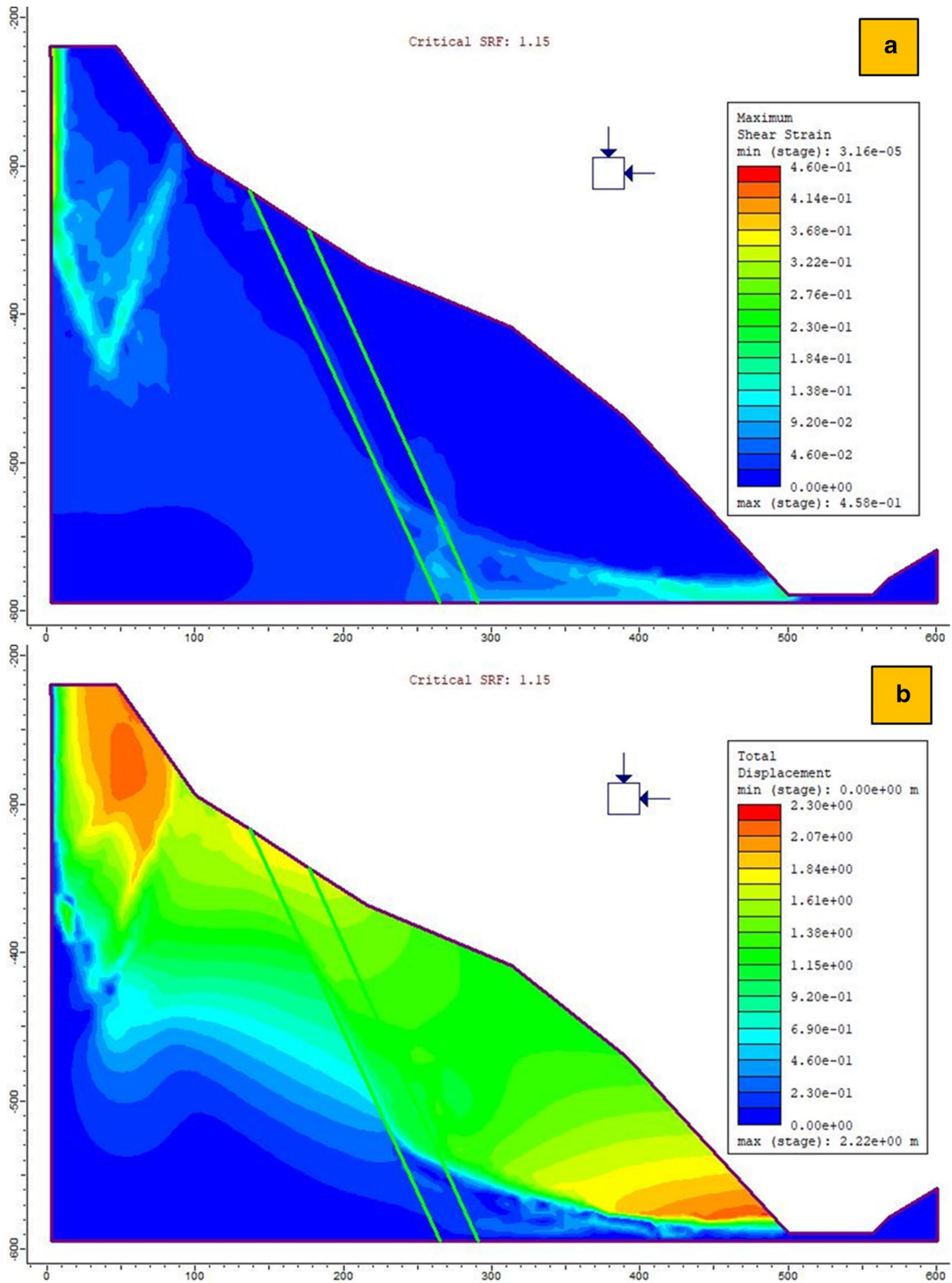


Fig. 16 **a** Pre-event finite element analysis for shear strain. **b** Finite element analysis for total displacement with maximum total displacement of 2.22 m

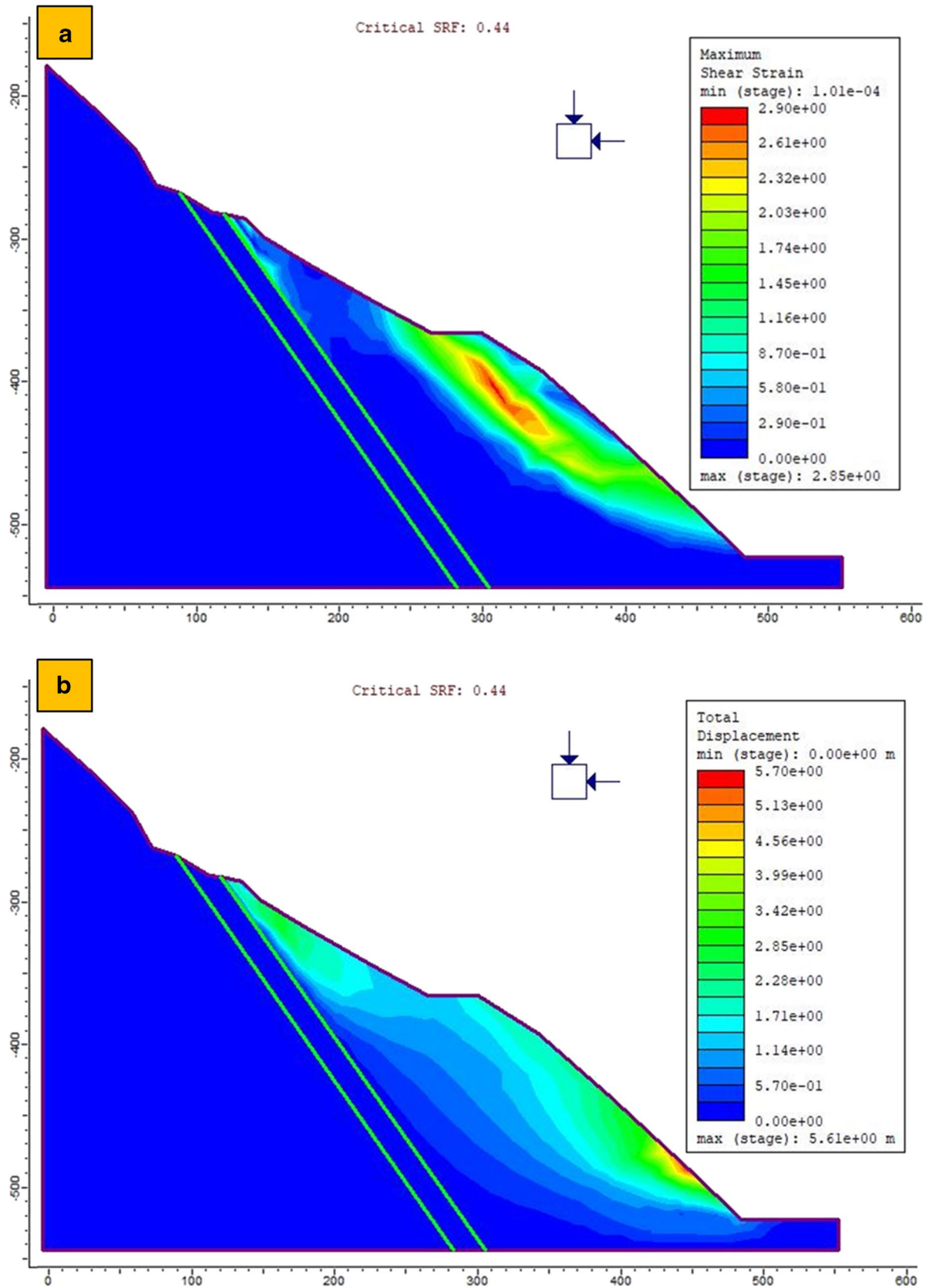


Fig. 17 **a** Post-event finite element analysis for shear strain. **b** Finite element analysis for total displacement with maximum total displacement of 5.61 m

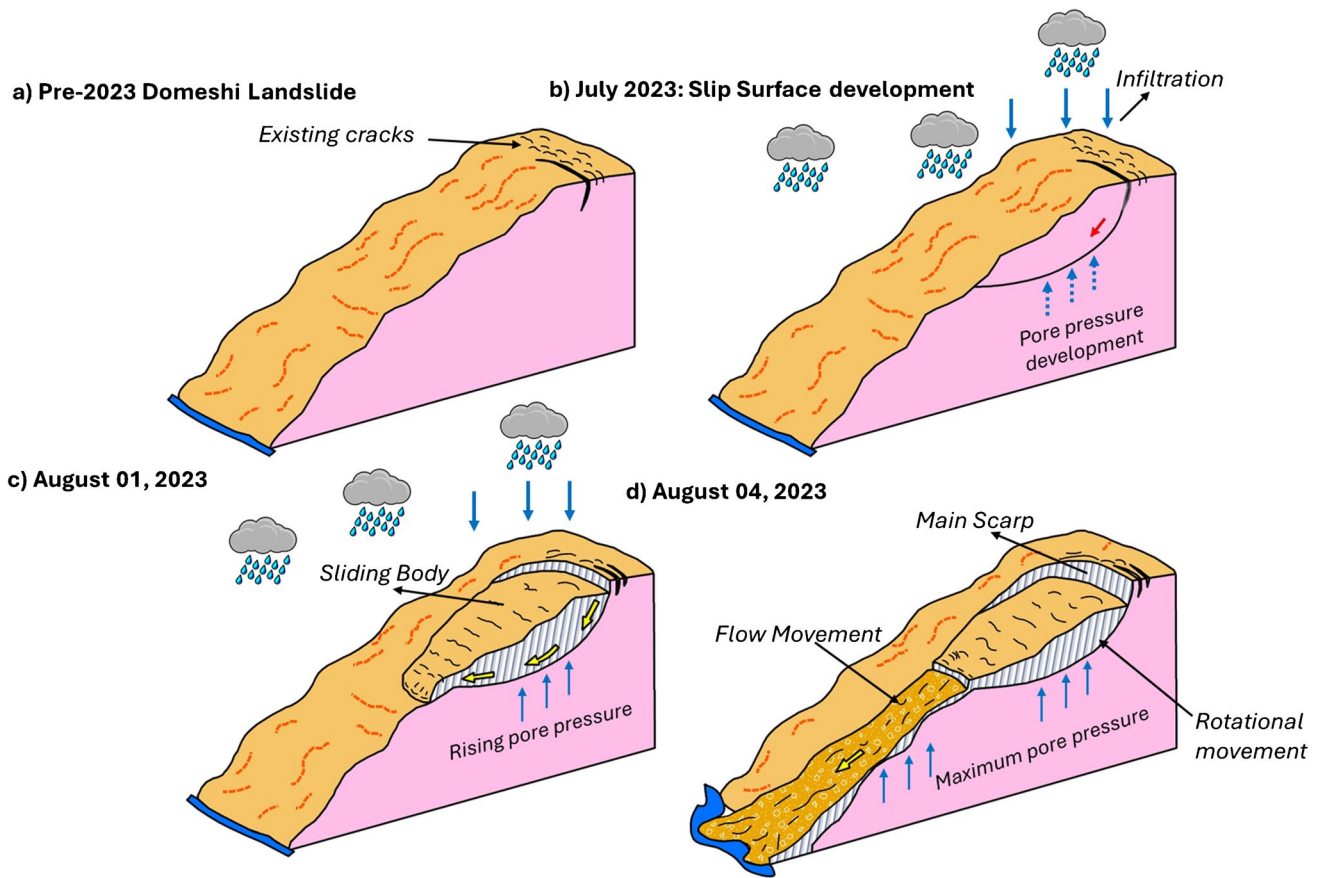


Fig. 18 Landslide conceptual model depicting landslide failure mechanism (adopted and modified from Sun et al. 2022)

particularly the dolomitic limestone and quartzite, making them more susceptible to failure (Riaz et al. 2023). The heterogeneous nature of the rock material contributed to the differential movement and internal deformation within the landslide mass (Willenberg et al. 2008).

3. **Unfavorable geological structure:** The geological configuration of the area also contributed to the slope failure (Aydan et al. 2009). The active JF cutting across the body of landslide had accelerated and intensified rock mass weakening. Field observations and petrographic examination showed microstructural features displaying pronounced shear forces affecting original rocks integrity. Such movement was facilitated by the orientation of bedding planes in rocks towards direction of landslide failure. Moreover, the presence of cracks and fractures in the rock mass allowed for the easy infiltration of rainwater, leading to increased porewater pressure and reduced shear strength.
4. **Rainfall:** The primary triggering factor for the Domeshi Landslide was the intense and prolonged rainfall experienced in July 2023. Rainfall data indicated that the area received 420 mm of rainfall, significantly higher than in the same period of previous years. This high amount of rainfall caused water to seep into the slope, enhancing saturation of the rock mass and increasing porewater pressure within landslide. The elevated pore pressure increased the effective stress in the rock mass, leading to a decrease in shear strength. The rock-water interac-

tion further deteriorated the shear strength of the rock mass, ultimately causing the slope to fail. The combination of large amounts of accumulated rainfall and high rainfall intensity were the most critical factors in triggering the landslide.

Lesson learnt

The comprehensive analyses of the Domeshi Landslide reveals a strong correlation between the strength and stiffness parameters of the soil and rock layers and the results from geotechnical and geophysical testing. The AMT survey identified the subsurface distribution of unconsolidated clays and deep consolidated rocks. These findings align with the mechanical sieve analysis, which showed a predominance of sand fractions contributing to increased infiltration and porewater pressure, and higher PI values along fault zone highlighting the role of clay content in soil weakening. The Proctor test further indicated that loose soils require significant compaction, correlating with their lower strength and higher compressibility. Direct shear test on rock samples demonstrated distinct fracture patterns under stress, with dolomitic limestone showing combined tension and shear deformation, and quartzite exhibiting brittle failure along quartz veins. The slope stability analysis, supported by these geotechnical parameters, consistently showed instability with a FoS less than 1, corroborating the geophysical

survey's identification of deep fractures and fault lines, such as the JF, as critical factors in the slope's destabilization.

The detailed study of landslide is important in an area where the material heterogeneity and the complex geologic structure are associated with driving mechanism of large-scale landslides (LaHusen and Grant 2024). Understanding this progression provides a unique opportunity to explore how triggering events such as extreme rainfall interact with pre-existing conditions to cause slope failure. This includes analyzing historical data such as satellite imagery from Google Earth, which showed past signs of instability including cracks and minor scarps that are key early warning signs for landslides. Due to 2005 Kashmir earthquake rock units are significantly decreased in strength. Detailed field observations and petrographic studies identified microstructural weaknesses, as well as illustrating the ways that geological structures such as fault or bedding planes influence slope stability. Furthermore, the case study underscored the importance of understanding hydrological factors, particularly how water infiltration and increased porewater pressure contribute to landslide activation. Several mitigation steps may be suggested to prevent landslides of the same nature. Better land use planning is necessary; buildings and agricultural activities need to be minimized in high-risk areas so that slopes are not disturbed further. Adherence to zoning regulations is important for slope stability. It is important to create and maintain dynamic rainfall-triggered landslide susceptibility maps. The maps can be used to inform land use planning and emergency response preparation. Empirical and physical based rainfall thresholds in relation to past observed events is necessary for the area affected by severe climatic conditions. In the area with poor network of rain gauges, a robust network of such gauges should be developed to track rainfall precisely in real time. Pairing such a network with an early warning system could alert communities and governments in time for them to take action.

Conclusions

The multi-faceted approach encompassing the geological, geomorphological, geotechnical, geophysical, and numerical methods has provided valuable insight into the fault-controlled Domeshe Landslide. Field investigations and petrographic analysis of rock units in the landslide demonstrate the intense deformation. Geomorphological analysis reveals that landslide has three distinct modes of failure including translational, rotational, and flow-like movement. The laboratory analysis reveals that high plasticity clays along fault planes played a crucial role in promoting significant volume changes, especially during and after rainfall events. A geophysical survey identified a layer of unconsolidated material up to the depth of 25 m, while multiple fractures including JF to a depth of 300 m highlighting the potential for deep-seated failure. The bedding joints were identified as the predominant failure planes oriented parallel to slope face. Kinematic analysis indicated planar and wedge types of failures with persistent failure potential in the future. Numerical modelling using LEM, FDM, and LEM revealed $FoS < 1$ highlighting that the slope is vulnerable to failure in the lower part of the landslide which can potentially originate a cascading geohazard in the form of a landslide dam. Our results highlight that rainfall is the main triggering factor of the landslide besides prevailing slope instability conditions as well as the presence of JF within

the landslide body, making it an ideal example of fault fault-controlled, rainfall-triggered complex landslide. The findings of the current study provide a comprehensive framework for landslide hazard evaluation for similar types of case studies in the region.

Acknowledgements

We gratefully acknowledge the support of the National Center of GIS and Space Applications (NCGSA) under Project No. RF-31-RS_GIS-15, for providing the funding for this research. Additionally, we acknowledge the contribution of the National Center of Excellence in Geology (NCEG), University of Peshawar, for generously providing UAV drone and preparation of rock core samples. We would also like to express our sincere gratitude to Bilal Kazmi, Raja Usama, Mr. Rizwan Akram, Mr. Naseem Ahmad, Mr. Ali Yousaf Khan, Mr. Ahmed Hammad Khaliq, and Dr. Mian Luqman Hussain for their valuable assistance during fieldwork.

Data Availability

Data used during the current study are available from the corresponding author on request.

Declarations

Competing interests The authors declare no competing interests.

References

- Ahmed KS, Basharat M, Riaz MT, Sarfraz Y, Shahzad A (2021) Geotechnical investigation and landslide susceptibility assessment along the Neelum road: a case study from Lesser Himalayas. Pakistan. Arab J Geosci 14(11):1019
- Aizawa K, Ogawa Y, Ishido T (2009) Groundwater flow and hydrothermal systems within volcanic edifices: Delineation by electric self-potential and magnetotellurics. J Geophys Res Solid Earth 114(B1)
- Ali A, Faisal S, Rehman K, Khan S, Ullah N (2015) Tectonic imprints of the Hazara Kashmir Syntaxis on the Northwest Himalayan fold and thrust belt, North Pakistan. Arab J Geosci 8:9857–9876
- Askarinejad A, Akca D, Springman SM (2018) Precursors of instability in a natural slope due to rainfall: a full-scale experiment. Landslides 15:1745–1759
- Askaripour M, Saeidi A, Mercier-Langevin P, Rouleau A (2022) A review of relationship between texture characteristic and mechanical properties of rock. Geotechnics 2(1):262–296
- Aydan Ö, Ohta Y, Hamada M (2009) Geotechnical evaluation of slope and ground failures during the 8 October 2005 Muzaffarabad earthquake, Pakistan. J Seismolog 13:399–413
- Barton N, Choubey V (1977) The shear strength of rock joints in theory and practice. Rockmechanics 10:1–54
- Basharat M, Riaz MT, Jan MQ, Xu C, Riaz S (2021) A review of landslides related to the 2005 Kashmir Earthquake: implication and future challenges. Nat Hazards 108:1–30
- Behr WM, Platt JP (2011) A naturally constrained stress profile through the middle crust in an extensional terrane. Earth Planet Sci Lett 303(3–4):181–192
- Blenkinsop TG (2007) Deformation microstructures and mechanisms in minerals and rocks. Springer Sci Bus Media
- Cappelli F, Costantini V, Consoli D (2021) The trap of climate change-induced “natural” disasters and inequality. Glob Environ Chang 70:102329

- Cheng YM, Lansivaara T, Wei WB (2007) Two-dimensional slope stability analysis by limit equilibrium and strength reduction methods. *Comput Geotech* 34(3):137-150
- Cygal A, Stefaniuk M, Kret A (2021) Integrated magnetotelluric and seismic investigation of Cenozoic graben structure near Obrzycko, Poland. *Acta Geophysica* 69(2):711-723
- Eckstein D, Künzel V, Schäfer L (2021) The global climate risk index 2021. Bonn: Germanwatch
- El Jazouli A, Barakat A, Khellouk R (2022) Geotechnical studies for Landslide susceptibility in the high basin of the Oum Er Rbia river (Morocco). *Geology, Ecology, and Landscapes* 6(1):40-47
- Farooq K, Rogers JD, Ahmed MF (2015) Effect of densification on the shear strength of landslide material: A Case Study from Salt Range, Pakistan. *Earth Science Research* 4(1):113
- Gariano SL, Guzzetti F (2016) Landslides in a Changing Climate. *Earth Science Reviews* 162:227-252
- Gómez D, García EF, Aristizábal E (2023) Spatial and temporal landslide distributions using global and open landslide databases. *Nat Hazards* 117(1):25-55
- Griffiths DV, Lane PA (1999) Slope stability analysis by finite elements. *Geotechnique* 49(3):387-403
- Hamasur GA (2022) Kinematic and Q-slope Application for Stability Assessment of the Rock Slopes Along Goshan_Qupy Qaradagh Road, Sulaimaniyah, NE-Iraq. *Jordan J Earth Environ Sci* 13(2)
- Hammah RE, Curran JH, Yacoub TE, Corkum B (2004) Stability analysis of rock slopes using the finite element method. In *Proceedings of the ISRM regional symposium EUROCK*
- Haque U, Da Silva PF, Devoli G, Pilz J, Zhao B, Khaloua A, Glass GE (2019) The human cost of global warming: Deadly landslides and their triggers (1995-2014). *Sci Total Environ* 682:673-684
- Hoek E (2005) *Rock Slope Engineering*, 4th edn. The Institute of Mining and Metallurgy, New York
- Hoek E, Bray JD (1981) *Rock slope engineering*. CRC Press
- Huang J, Ma C, Sun Y (2021) 2D Magnetotelluric forward modelling for deep buried water-rich fault and its application. *J Appl Geophys* 192:104403
- Hufschmidt G, Crozier M, Glade T (2005) Evolution of natural risk: research framework and perspectives. *Nat Hazard* 5(3):375-387
- Jiang S, Meng J, Zhu L, Cheng H (2021) Spatial-temporal pattern of land use conflict in China and its multilevel driving mechanisms. *Sci Total Environ* 801:149697
- Khabbaz H, Fatahi B, Nucifora C (2012) Finite element methods against limit equilibrium approaches for slope stability analysis. In *Australia New Zealand Conference on Geomechanics*. Geomech Soc New Zealand Geotech Soc
- Khan MA, Basharat M, Riaz MT, Sarfraz Y, Farooq M, Khan AY, Shahzad A (2021) An integrated geotechnical and geophysical investigation of a catastrophic landslide in the Northeast Himalayas of Pakistan. *Geolog J* 56(9):4760-4778
- Khan AY, Niaz A, Nisar UB (2024) Multi-dimensional characterization of groundwater distribution in sub-Himalayan region of Pakistan. *Environ Earth Sci* 83(2):64
- Khattak GA, Owen LA, Kamp U, Harp EL (2010) Evolution of earthquake-triggered landslides in the Kashmir Himalaya, northern Pakistan. *Geomorphology* 115(1-2):102-108
- Kiani UBN, Najam FA, Rana IA (2022) The impact of risk perception on earthquake preparedness: An empirical study from Rawalakot. *Pakistan International Journal of Disaster Risk Reduction* 76:102989
- Kinde M, Getahun E, Jothimani M (2024) Geotechnical and slope stability analysis in the landslide-prone area: A case study in Sawla-Laska road sector. *Southern Ethiopia Scientific African* 23:e02071
- Kitutu MG, Muwanga A, Poesen J, Deckers JA (2009) Influence of soil properties on landslide occurrences in Bududa district, Eastern Uganda. *African Journal of Agricultural Research* 4(7):611-620
- Kliche CA (1999) *Rock slope stability*. Society for Mining, Metallurgy, and Exploration, Inc., Littleton
- Knapen A, Kitutu MG, Poesen J, Breugelmans W, Deckers J, Muwanga A (2006) Landslides in a densely populated county at the footslopes of Mount Elgon (Uganda): characteristics and causal factors. *Geomorphology* 73(1-2):149-165
- Lacroix P, Handwerker AL, Bièvre G (2020) Life and death of slow-moving landslides. *Nature Reviews Earth & Environment* 1(8):404-419
- LaHusen SR, Grant AR (2024) Complex landslide patterns explained by local intra-unit variability of stratigraphy and structure: Case study in the Tyee Formation, Oregon, USA. *Eng Geol* 329:107387
- Li Z, Shi J, Tang A (2017) An investigation of failure modes and failure criteria of rock in complex stress states. *Journal of the Southern African Institute of Mining and Metallurgy* 117(3):245-255
- Li W, An X, Li H (2018) Limestone mechanical deformation behavior and failure mechanisms: a review. *Acta Geochimica* 37:153-170
- Lisabeth HP, Zhu W (2015) Effect of temperature and pore fluid on the strength of porous limestone. *Journal of Geophysical Research: Solid Earth* 120(9):6191-6208
- Liu SY, Shao LT, Li HJ (2015) Slope stability analysis using the limit equilibrium method and two finite element methods. *Comput Geotech* 63:291-298
- Liu Q, Tian Y, Liu D, Jiang Y (2017) Updates to JRC-JCS model for estimating the peak shear strength of rock joints based on quantified surface description. *Engineering Geology* 228:282-300
- Ma S, Yao Y, Bao P, Guo C (2023) Effects of moisture content on strength and compression properties of foundation soils of cultural relics in areas flooded by the Yellow River. *Frontiers in Materials* 10:1186750
- Mebrahtu TK, Heinze T, Wohnlich S, Alber M (2022) Slope stability analysis of deep-seated landslides using limit equilibrium and finite element methods in Debre Sina area, Ethiopia. *Bull Eng Geol Env* 81(10):403
- Mekkawi MM, Abd-El-Nabi SH, Farag KS, Abd Elhamid MY (2022) Geothermal resources prospecting using magnetotelluric and magnetic methods at Al Ain Al Sukhuna Al Galala Al Bahariya area, Gulf of Suez. *Egypt Journal of African Earth Sciences* 190:104522
- Mezzerreg NEH, Kessasra F, Boufouha Y, Bouabdallah H, Bollot N, Baghdad A, Bougdal R (2019) Integrated geotechnical and geophysical investigations in a landslide site at Jijel, Algeria. *Journal of African Earth Sciences* 160:103633
- Mona Lisa, Khawaja, A. A. (2004) Structural trends and focal mechanism studies in the Potwar area with special emphasis on hydrocarbon exploration. *Pak. Jour Hydroc Rec* 14:49-59
- Moussadek R, Laghrou M, Mrabet R, Van Ranst E, Badraoui M, Mekkaoui M (2017) Morocco's vertisol characterization (tirs). *JOURNAL OF MATERIALS & ENVIRONMENTAL SCIENCE* 8(11):3932-3942
- Mugaga F, Kakembo V, Buyinza M (2012) A characterisation of the physical properties of soil and the implications for landslide occurrence on the slopes of Mount Elgon, Eastern Uganda. *Nat Hazards* 60:1113-1131
- Mukasa-Tebandeke IZ, Ssebuwufu PJM, Nyanzi SA, Schumann A, Nyakairu GWA, Ntale M, Lugolobi F (2015) The elemental, mineralogical, IR, DTA and XRD analyses characterized clays and clay minerals of Central and Eastern Uganda
- Mukherjee S, Tayade L (2019) Kinematic analyses of brittle rotational planar and listric faults based on various rotational to translational velocities of the faulted blocks. *Mar Pet Geol* 107:326-333
- Oyediran IA, Durojaiye HF (2011) Variability in the geotechnical properties of some residual clay soils from southwestern Nigeria. *Int J Sci Eng Res* 2(9):1-6
- Ozbay A, Cabalar AF (2015) FEM and LEM stability analyses of the fatal landslides at Çöllolar open-cast lignite mine in Elbistan, Turkey. *Landslides* 12:155-163

- Panwar V, Sen S (2019) Economic impact of natural disasters: An empirical reexamination. *Margin J Appl Econom Res* 13(1):109–139
- Pasierb B, Grodecki M, Gwóźdz R (2019) Geophysical and geotechnical approach to landslide stability assessment: a case study. *Acta Geophys* 67(6):1823–1834
- Peng M, Wang X, Zhang G, Veh G, Sattar A, Chen W, Allen S (2023) Cascading hazards from two recent glacial lake outburst floods in the Nyainqentanglha range. *Tibetan Plateau Journal of Hydrology* 626:130155
- Petley DN, Dunning SA, Rosser NJ (2005) The analysis of global landslide risk through the creation of a database of worldwide landslide fatalities. In *Landslide risk management* (pp. 377–384). CRC Press
- Pourkhosravani A, Kalantari B (2011) A review of current methods for slope stability evaluation. *Electron J Geotech Eng* 16:1245–1254
- Quevedo RP, Velastegui-Montoya A, Montalván-Burbano N, Morante-Carballo F, Korup O, Daleles Rennó C (2023) Land use and land cover as a conditioning factor in landslide susceptibility: a literature review. *Landslides* 20(5):967–982
- Rahman AU, Zhang G, AlQahtani A, S., Janjuhah, H. T., Hussain, I., Rehman, H. U., & Shah, L. A. (2023) Geotechnical assessment of rock slope stability using kinematic and limitequilibrium analysis for safety evaluation. *Water* 15(10):1924
- Riaz MT, Basharat M, Hameed N, Shafique M, Luo J (2018) A data-driven approach to landslide-susceptibility mapping in mountainous terrain: case study from the Northwest Himalayas. *Pakistan Natural Hazards Review* 19(4):05018007
- Riaz S, Wang G, Basharat M, Takara K (2019) Experimental investigation of a catastrophic landslide in northern Pakistan. *Landslides* 16:2017–2032
- Riaz MT, Basharat M, Pham QB, Sarfraz Y, Shahzad A, Ahmed KS, Waseem MH (2022) Improvement of the predictive performance of landslide mapping models in mountainous terrains using cluster sampling. *Geocarto Int* 37(26):1229412337
- Riaz MT, Basharat M, Brunetti MT (2023) Assessing the effectiveness of alternative landslide partitioning in machine learning methods for landslide prediction in the complex Himalayan terrain. *Progress in Physical Geography: Earth and Environment* 47(3):315347
- Sabin TP, Krishnan R, Vellore R, Priya P, Borgaonkar HP, Singh BB, Sagar A (2020) Climate change over the Himalayas. Assessment of climate change over the Indian region: A report of the Ministry of Earth Sciences (MoES), Government of India, 207–222
- Safi I, Rehman G, Yaseen M, Wahid S, Nouman M, Fida S, Anjum MN (2021) Effects of transpression on the rocks exposed at the Jhelum Fault Zone in the east of Potwar Basin, Pakistan: implications on the subsurface deformation pattern. *J Petrol Explor Product Technol* 11:2407–2424
- Santangelo M, Althuwaynee O, Alvioli M, Ardizzone F, Bianchi C, Bor-naetxea T, Fiorucci F (2023) Inventory of landslides triggered by an extreme rainfall event in Marche-Umbria, Italy, on 15 September 2022. *Sci Data* 10(1):427
- Sari M (2019) Stability analysis of cut slopes using empirical, kinematical, numerical and limitequilibrium methods: case of old Jeddah-Mecca road (Saudi Arabia). *Environmental Earth-Sciences* 78(21):621
- Shabbir W, Omer T, Pilz J (2023) The impact of environmental change on landslides, fatallandslides, and their triggers in Pakistan (2003–2019). *Environmental Science and Pollution Research* 30(12):33819–33832
- Shaheen AUH, Ahmed KS, Sarfraz Y, Riaz MT, Shahzad A (2023) Physicomechanical characterization of cement concrete using quarry waste as fine aggregate replacement of natural sand. *Arab J Sci Eng* 48(10):13807–13821
- Shahzad A, Kontakiotis G, Adatte T, Ahmed KS, Riaz MT, Janjuhah HT, Besiou E (2024) Multi-elemental chemostratigraphy, sequence development, depositional history, and environmental importance of early Eocene red beds (Kuldana Formation) in NW Himalayas Pakistan. *J Earth Sci* 35(2):349–375
- Sharma M, Sharma S, Kumar M, Singh SK (2019) Analysis of slope stability of road cut slopes of Srinagar, Uttrakhand. *India Int J Appl Eng Res* 14(3):609–615
- Sim KB, Lee ML, Wong SY (2022) A review of landslide acceptable risk and tolerable risk. *Geoenvironmental Disasters* 9(1):3
- Soeters R, Van Westen CJ (1996) Slope instability recognition, analysis and zonation. *Landslides: Investigation and Mitigation* 247:129–177
- Soren K, Budi G, Sen P (2014) Stability analysis of open pit slope by finite difference method. *Int J Res Eng Technol* 3(5):326–334
- Srivastava V, Mukul M, Barnes JB (2016) Main Frontal thrust deformation and topographic growth of the Mohand Range, northwest Himalaya. *Journal of Structural Geology* 93:131–148
- Stianson JR, Chan D, Fredlund DG (2015) Role of admissibility criteria in limitequilibrium slope stability methods based on finite element stresses. *Computers and Geotechnics* 66:113–125
- Stipp M, Tullis J, Scherwath M, Behrmann JH (2010) A new perspective on paleopiezometry: Dynamically recrystallized grain size distributions indicate mechanism changes. *Geology* 38(8):759–762
- Sun SW, Liu L, Hu JB, Ding H (2022) Failure characteristics and mechanism of a rain-triggered landslide in the northern longwall of Fushun west open pit. *China Landslides* 19(10):2439–2458
- Tang G, Huang J, Sheng D, Sloan SW (2018) Stability analysis of unsaturated soil slopes under random rainfall patterns. *Eng Geol* 245:322–332
- Thomas V (2017) Climate change and natural disasters: Transforming economies and policies for a sustainable future (p. 158). Taylor & Francis
- Tiwari B, Ajmera B (2011) A new correlation relating the shear strength of reconstituted soil to the proportions of clay minerals and plasticity characteristics. *Applied Clay Science* 53(1):48–57
- Tiwari B, Ajmera B (2023) Advancements in shear strength interpretation, testing, and use for landslide analysis. In *Progress in Landslide Research and Technology, Volume 2 Issue 2, 2023* (pp. 3–54). Cham: Springer Nature Switzerland
- Truty A, Urbański A, Grodecki M, Podleś K (2009) Computer aided models of landslides and their protection problems. Polish with English and German summary). *Scientific technical papers of communication engineers and technicians of the Republic of Poland in Cracow* 88(144):395–419
- Turab SA (2012) Structural geology of the surrounding of Muzaffarabad with emphasis of Neotectonics (Doctoral dissertation). Thesis, National Centre of Excellence in Geology, University of Peshawar, M. Phil
- Vinod BR, Shivananda P, Swathivarman R, Bhaskar MB (2017) Some of limitequilibrium method and finite element method based software are used in slope stability analysis. *IJAIEEM* 6(9):6–10
- Wang HM, Cao L, Yao J, Li Z (2013) The application of FLAC software in stability analysis of highway slope reinforced by prestressed anchor cable. *Applied Mechanics and Materials* 241:2158–2162
- Wang H, Sun P, Zhang S, Han S, Li X, Wang T, Xin P (2020) Rainfall-induced landslide in loess area, Northwest China: a case study of the Change landslide on September 14, 2019, in Gansu Province. *Landslides* 17:2145–2160
- Wang F, Chen Y, Peng X, Zhu G, Yan K, Ye Z (2022) The fault-controlled Chengtian landslide triggered by rainfall on 20 May 2021 in Songyang County, Zhejiang Province. *China Landslides* 19(7):1751–1765
- Wati SE, Hastuti T, Widjojo S, Pinem F (2010) Landslide susceptibility mapping with heuristic approach in mountainous area: A case study in Tawangmangu sub district Central Java,

- Indonesia. *International Archives of the Photogrammetry, Remote Sensing and Spatial Information Science* 38(Part 8)
- Willenberg H, Loew S, Eberhardt E, Evans KF, Spillmann T, Heincke B, Green AG (2008) Internal structure and deformation of an unstable crystalline rock mass above Randa (Switzerland): Part I—Internal structure from integrated geological and geophysical investigations. *Eng Geol* 101(1–2):1–14
- Wilson CJL, Hunter NJR, Luzin V (2022) Crystallographic preferred orientation of quartz deformed at granulite conditions: the Kalinjala Shear Zone, Port Neill. South Australia Australian Journal of Earth Sciences 69(8):1119–1131
- Wyllie DC, Mah WC (2004) *Rock Slope Engineering*, 4th edn. Taylor & Francis Group, New York
- Wysokiński L (2011) The methods of landslides prediction and their protection. In XXV scientific conference “Building failures (pp. 291–320)
- Xu JS, Yang XL (2018) Three-dimensional stability analysis of slope in unsaturated soils considering strength nonlinearity under water drawdown. *Eng Geol* 237:102115
- Xu Z, Li G, Xin H, Tang J, Lv F (2020) Hydrogeological prospecting in the Da Qaidam area of the Qaidam Basin using the audio-frequency magnetotelluric method. *Journal of Applied Geophysics* 182:104179
- Yalcin A (2011) A geotechnical study on the landslides in the Trabzon Province, NE. Turkey *Applied Clay Science* 52(1–2):11–19
- Yusuf SN, Wamtas IG, Imagbe LO, Yohanna OM (2022) *Science Forum. J Pure Appl Sci* 22:541–549
- Zein AKM, Karim WA (2017) Stability of slopes on clays of variable strength by limit equilibrium and finite element analysis methods. *GEOMATE Journal* 13(38):157–164
- Zhang S, Li C, Zhang L, Peng M, Zhan L, Xu Q (2020) Quantification of human vulnerability to earthquake-induced landslides using Bayesian network. *Engineering Geology* 265:105436

Springer Nature or its licensor (e.g. a society or other partner) holds exclusive rights to this article under a publishing agreement with the author(s) or other rightsholder(s); author self-archiving of the accepted manuscript version of this article is solely governed by the terms of such publishing agreement and applicable law.

Muhammad Tayyib Riaz (✉) · **Muhammad Basharat · Khawaja Shoaib Ahmed · Yasir Sirfraz · Amir Shahzad**

Institute of Geology, University of Azad Jammu and Kashmir, Muzaffarabad 13100, Pakistan

Muhammad Tayyib Riaz

Email: tayyibriaz@yahoo.com

Nisar Ali Shah

National Centre of Excellence in Geology, University of Peshawar, Peshawar, Pakistan